Equilibrium Configurations of Hexagonal Columnar Liquid Crystals with Applications to Materials Science and Biology

A DISSERTATION
SUBMITTED TO THE FACULTY OF THE
UNIVERSITY OF MINNESOTA
BY

Lindsey Hiltner

IN PARTIAL FULFILLMENT OF THE REQUIREMENTS
FOR THE DEGREE OF
DOCTOR OF PHILOSOPHY

Dr. Maria-Carme Calderer

November 2018

Abstract

Using the mathematical theory of liquid crystals, we propose models for equilibrium configurations of the hexagonal columnar phase of lyotropic chromonic liquid crystals (LCLCs). These models are applied in a collection of settings in which the underlying phases are naturally observed, including LCLC toroidal superstructures, liquid crystal confined to a thin capillary, double-stranded DNA packed in bacteriophage viruses, and DNA toroidal clusters that form in the presence of condensing agents. Although the length scale of these superstructures ranges from nanometers to microns, they show the ability to sustain pressures of up to 60 atmospheres. In each setting, we investigate equilibrium configurations and discuss well-posedness of our model. The mathematical work focuses in the analysis of constrained free boundary problems for combined liquid crystal and elastic energies, with a main focus on the very rich structure of defect cores in lyotropic systems. We conclude with potential modifications to the model that could be used to incorporate information such as ionic concentrations present in the medium surrounding this liquid crystal phase.

Table of Contents

List of Tables

List of Figures

1 Introduction

Scientific exploration of soft matter has resulted in numerous industry-changing technologies such as the bulletproof polymer Kevlar, the widely used liquid crystal displays, and development of new approaches to drug delivery, nano-templated materials, and colloidal systems. In order to further develop fundamental science and technologies of the future, it is pivotal to learn how to design, produce, and control the structure, properties, and dynamic behavior of soft materials within a broad range of spatial length scales, from the nanometer scale to macroscale. The ability of soft matter to form a plethora of complex and functional structures with tunable local and non-local responses to external excitation can easily be exploited once well understood. This dissertation focuses on the properties of the so-called lyotropic chromonic liquid crystals, a material whose properties are shared with many systems of interest, such as condensed DNA and the spooling of double-stranded DNA in viruses that attack bacteria known as bacteriophages. More generally, the chromonic liquid crystal family embraces a very broad range of materials, examples of which are abundant and include nucleotides, DNA and RNA, dyes and food additives (e.g. the dye Sunset Yellow), proteins, and pharmaceutical products [40, 60].

The goal of this dissertation is the study of equilibrium configurations of chromonic liquid crystals, with a main emphasis in the mathematical features of their defect cores. The analysis of constrained free boundary problems for chromonic clusters is central to the present work. These include mathematical studies of packing of the DNA of bacteriophage viruses, showing that the spooling configuration present in nature is the one with minimum energy.

Lyotropic chromonic liquid crystals (LCLCs) differ dramatically from the typical liquid crystals found in displays, which have long, rod-like molecules and change phase at well known temperature thresholds. When it comes to LCLCs, which consist of water-soluble, plank-like molecules with rigid cores and ionic groups at the periphery that can reversibly assemble into columns by stacking face to face, the length of these columnar aggregates varies strongly with temperature, concentration, and ionic content [65]. As the concentration of these molecules increases, the columns tend to elongate and align parallel, forming a columnar nematic phase. As the concentration further increases, the more organized hexagonal columnar phase appears with the long axes of the columns forming a two-dimensional hexagonal lattice (see Figure 1). With the addition of condensing agents, the columns rearrange into toroidal aggregates.

The tendency of LCLC molecules to form macromolecules at high concentrations or in the presence of certain condensing agents gives rise to complex structures, with properties defined by a fine balance of anisotropic surface tension and anisotropic bulk elasticity. Shapes of these superstructures include tactoids and toroids, with typical size on the order of 200 microns with pressures around 0.1 atmospheres, that are seen to coexist with the disordered isotropic state [60], shown

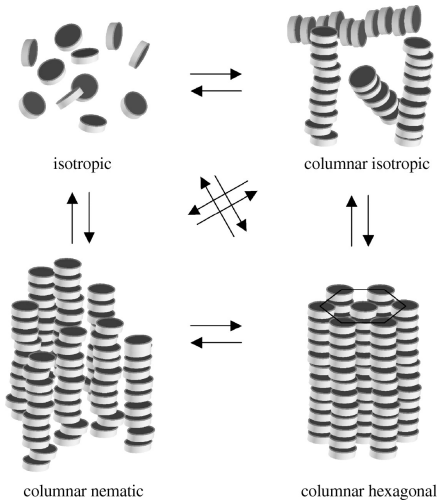

Figure 1: Phases of a chromonic liquid crystal

in Figure 2. The toroids form, for example, by groups of six columns bundling together in a honeycomb formation then folding around so that their two ends meet. Double-stranded DNA in free solution forms toroidal aggregates in the presence of condensing agents, but with clusters of sizes five orders of magnitude smaller than those formed by the LCLC and anti-asthmatic drug known as DSCG. Another important natural setting in which the hexagonal columnar structure is exhibited is in bacteriophage viruses, where the DNA is tightly packed within.

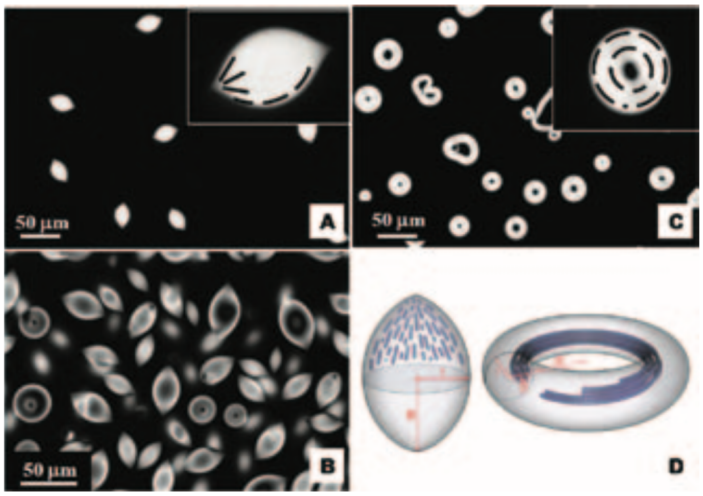

Figure 2: Phase separation of an LCLC with increasing amount of additives, taken from [59]: (A) Nematic tactoids (B) coexisting tactoids and toroids (C) Columnar toroids (D) scheme of director distortions inside a tactoid and a toroid

In the case of bacteriophages, viruses that invade bacteria, very little is known or understood about how they carry, eject, or replicate their DNA. These viruses consist of a protein shell called a capsid

and a tail with protein receptors. The life cycle of bacteriophages begins when DNA is spooled into an early form of capsid using a molecular motor while still in a bacterial host cell. The fully formed bacteriophages then destroy the host and leave to seek a live bacterium in which to replicate. Once the receptors on the tail detect a viable host, a reaction occurs that causes the DNA to be injected into the host, using the built up pressure within to release it. The bacteriophages take over the DNA replication mechanism of the host and copy their own DNA, which occurs rapidly since the viruses have much smaller genomes than the mechanism is made to handle, and the process begins again.

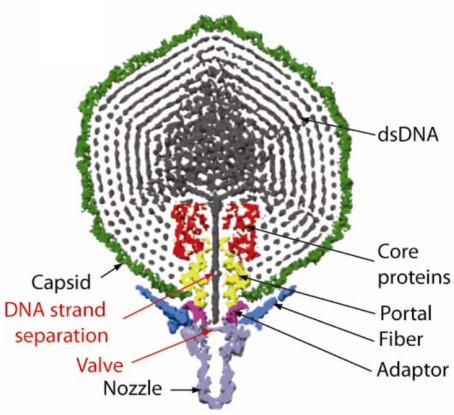

Figure 3: Image of a bacteriophage, taken from [51]

Bacteriophages are unique in that, with few exceptions, only their genome enters the host cell; in almost all other viruses the entire virus structure enters the cell cytoplasm [61]. This suggests that the DNA within the bacteriophage capsid must be optimally packed for ejection, with pressures strong enough to inject the genome into the host cell. Typical bacteriophages measure about 50 nm in diameter and sustain internal pressures of around 30 to 60 atmospheres, much greater than the pressure within a corked bottle of champagne at about 10 atmospheres. This build up of pressure is caused by the confinement imposed on the DNA by the capsid, the bending rigidity of the DNA strand, and the electrostatic self-repulsion between the highly negatively charged DNA segments. Thus, understanding the arrangement of DNA inside a viral capsid is a key step in developing predictive models of bacteriophage genome delivery.

It is predicted that technologies using phages – such as delivering genes that cause toxicity to target cells, inhibiting bacterial processes like replication, and detecting pathogens in hospital surfaces and food preparation – could aid or replace antibiotics in impeding highly resistant strains of disease causing bacteria [10]. With the number of potential applications of both naturally-occurring and synthesized bacteriophages growing every day, the ability to understand, accurately describe, and simulate certain phenomena associated to these objects is of increasing interest. For this reason, the development of mathematical models that describe the features of bacteriophages will prove to be

very useful.

Many mathematical models have been proposed to describe the packing of DNA in viruses [2, 28, 41, 50, 61] with energy functionals borrowed from the study of DNA molecules in free solution that do not account for possible liquid crystalline phases. It has been seen that confined DNA exhibits liquid crystalline structure, in particular, the segments of spooled DNA act as the columns described above and form a hexagonal lattice [35, 41, 43]. In fact, the denomination of *chromonic* comes directly from the discovery that DNA (i.e. chromosomes) form liquid crystal phases. Therefore, we present a continuum model for DNA encapsidation using the theory of chromonic liquid crystals, which has long been used in the study of biological systems [55].

The utility of a well-tuned continuum model includes the ability to accurately and reproducibly predict features of the system, such as pressure within a capsid, equilibrium shapes of aggregates, or the amount of disordered material coexisting with ordered material. Thus, one of the main goals of this dissertation is to thoroughly study the *predictive* capabilities of the proposed models in relevant geometries and settings, ensuring that our model is describing the important features of the physical systems. With that goal in mind, the ability to tune parameters of the model becomes important.

The energy density of a chromonic liquid crystal includes the Oseen-Frank energy of the nematic liquid crystal phase that penalizes bending of the columns, together with an elastic energy that accounts for distortions of the cross-sectional lattice perpendicular to the columnar directions at each point of the domain. Chromonic configurations are described by a set of linearly independent unit vectors, $\mathbf{n}$, $\mathbf{m}$ and $\mathbf{p}$. The nematic director $\mathbf{n}$ represents the average direction of column arrays at a point, and $\mathbf{m}$ and $\mathbf{p}$ denote the lattice vectors of the local cross-section.

As in the modeling of rigid rod systems, defects correspond to points, lines, or surfaces with $\mathbf{n} = \mathbf{0}$, that is where the order is lost, with the material becoming locally isotropic. Studies of liquid crystal defects span nearly a hundred years of research with several theories involved. The main difficulty with the Oseen-Frank theory, one of the first and most widely used in the description of equilibrium as well as flow configurations of nematics, is in the modeling of two-dimensional configurations since it assigns infinite energy to point defects in the plane. Our focus on three-dimensional configurations allows us to postulate and analyze such an energy as part of our studies of chromonic clustering. The proposed elastic energy to model distortions of the columnar cross-sections is motivated by that proposed by de Gennes [21] and formulated in terms of deformation gradients. Following the approach employed in the study of solid crystals, we write the former in terms of gradients of the lattice vectors $\mathbf{m}$ and $\mathbf{p}$. The resulting expression then involves the bulk and shear moduli of the chromonic material. The proposed energy to describe clusters also includes the penalty associated with the isotropic core and the surface energy of the interface between the ordered and the disordered part of the configuration. In the case of the bacteriophage viruses, information on the disordered core is obtained from the cryogenic electron microscopy images.

A main difference between rod and disk-like liquid crystals is on the size of their cores. Whereas fractions of nanometers characterize the former, chromonic cores can be on the order of 10 microns. A main goal of this thesis is the study of core defects in chromonics found in experiments with materials such as Sunset Yellow and the anti-asthmatic drug disodium cromoglycate/water system. The analysis presented in the dissertation involves three types of systems: toroidal clusters of DNA and Sunset Yellow, defects in capillary domains of the latter, and packing of the DNA genome of bacteriophage viruses.

The analysis addresses the minimization of the packing energies subject to multiple constraints. These lead to free boundary problems for polyconvex energy functionals. The constraints involved are of geometric type, including those that reflect the rigidity of the material to splay and twist deformations, the hexagonal structure of the lattice, and the conservation of mass. The elastic energy is particularly relevant to the modeling of DNA encapsidation, due to the polymeric structure of the DNA molecule, with persistence length of the same order of magnitude as the capsid size. The capsid is taken to be an axisymmetric domain, neglecting its polyhedral structure. Although some viruses present a chiral arrangement, this analysis focuses on standard spooling configurations around the capsid axis. In fact, it is found that among configurations of interest that the planar spooling configuration is the minimizer. The shape of the core depends on the physical parameters of the model, and in particular, the bending rigidity of the DNA.

It is also true of liquid crystal confined to a capillary and of toroidal aggregates that the relative significance of surface forces between adjacent phases, when compared to the bending contribution to the energy, is a key feature in determining equilibrium shapes. In both the capillary and toroid cases, both regimes are considered, demonstrating that with some calibration of the constants of the model, that a desired configuration can be achieved. A bifurcation study is conducted in the capillary setting, in which we assume ordered material is confined between coaxial cylinders and a disordered phase exists within the central cylinder, to find both the size of the inner cylinder radius and the ratio of surface tension and bending parameters that distinguish between a planar or twist equilibrium state of the liquid crystal. In the toroid, we first analyze limiting cases in which either the bending or surface tension is the main contributor to the energy, then compute examples of equilibrium shapes in each setting based on experimental measurements. We use experimental work on chromonic liquid crystals in the case where surface tension dominates, and consider DNA toroidal shapes when bending dominates.

This dissertation is organized in the following way. In Section 2, we outline the process used in proving the existence of minimizers and give the necessary results for both generic functionals and for the Oseen-Frank energy functional from liquid crystal theory. We present our basic model for configurations of hexagonal columnar LCLCs in Section 3. A modified model for DNA packed in a bacteriophage capsid is presented in Section 4, as well as a explanation of prior work in this area,

describing the location of the DNA filament, and accounting for the self-repulsion of the spooled DNA. We go on to investigate equilibrium shapes of these materials in Sections 6 and 7, where the mathematical results on the well-posedness of the model in these geometries are also proved. Section 8 that describes expansions of the model to incorporate concentrations of condensing agents and effects of ionic concentrations. The paper closes with concluding remarks in Section 9.

2 Background Materials

2.1 Calculus of Variations

In this section, we lay out the roadmap used to prove the existence of minimizers of a functional, which will imply well-posedness of the models proposed in this work. We discuss the notions of coercivity, compactness, weak lower semicontinuity, and convexity.

We give definitions and theory used in showing the existence of minimizers of a functional defined by

$$I[w] := \int_\Omega L(\nabla w(x), w(x), x)\, dx,$$

for appropriate $w : \Omega \to \mathbb{R}$ satisfying $w = g$ on $\partial\Omega$ for some given function g. The results are stated and proved in the scalar case, but also hold in the case of vector fields, with

$$I[\mathbf{w}] := \int_\Omega L(\nabla \mathbf{w}(x), \mathbf{w}(x), x)\, dx,$$

unless noted otherwise.

Definition 1. *We call a function coercive if there exist constants $\alpha > 0,\ \beta \geq 0$, and fixed $1 < q < \infty$ such that*

$$L(p, z, x) \geq \alpha|p|^q - \beta,$$

for all $p \in \mathbb{R}^n,\ z \in \mathbb{R},\ x \in \Omega$.

This implies

$$I[w] \geq \delta\|\nabla w\|^q_{L^q(\Omega)} - \gamma. \tag{1}$$

From inequality (1), it becomes reasonable to search for minimizers in $W^{1,q}(\Omega)$ that satisfy the

boundary condition in the trace sense. Therefore, we can search for minimizers in the class

$$\mathcal{A} = \{w \in W^{1,q}(\Omega) \ : \ \text{trace}(w) = g\}. \tag{2}$$

In general, coercivity is not enough to guarantee the existence of a minimizer of the functional I. This becomes an issue when we consider the following.

Set $m := \inf_{w \in \mathcal{A}} I[w]$ and choose a sequence $\{u_k\} \subset \mathcal{A}$ such that

$$I[u_k] \to m \quad \text{as } k \to \infty.$$

We call $\{u_k\}$ a minimizing sequence. Due to the infinite dimensionality of $W^{1,q}(\Omega)$, we do not have the compactness to conclude that there exists a subsequence that converges to a minimizer in $W^{1,q}(\Omega)$.

Therefore, again assuming $1 < q < \infty$ so that $L^q(\Omega)$ is reflexive, then there exists a subsequence $\{u_{k_j}\} \subseteq \{u_k\}$ and a function $u \in W^{1,q}(\Omega)$ so that

$$\begin{aligned} u_{k_j} &\rightharpoonup u \text{ in } L^q(\Omega), \\ \nabla u_{k_j} &\rightharpoonup \nabla u \text{ in } L^q(\Omega). \end{aligned}$$

Also, it will be true that $u = g$ on $\partial\Omega$ in the trace sense, so $u \in \mathcal{A}$.

Now that we consider sequences in the weak topology, there is enough compactness from (1) to deduce there is a weakly convergent subsequence. The last hurdle is that I is not continuous with respect to weak convergence, so we cannot deduce that

$$I[u] = \lim_{j \to \infty} I[u_{k_j}],$$

which would imply u is a minimizer. It would suffice to know that the following definition holds.

Definition 2. *We say a functional I is weak lower semicontinuous on $W^{1,q}(\Omega)$ if whenever $u_k \rightharpoonup u$ in $W^{1,q}(\Omega)$ then*

$$I[u] \leq \liminf_{k \to \infty} I[u_k]. \tag{3}$$

The next thing to do is identify reasonable conditions on the nonlinear term L to ensure I is weak

lower semicontinuous. Looking at the second variation, we find that

$$\sum_{i,j=1}^{n} L_{p_i p_j}(\nabla u, u, x)\xi_i \xi_j \geq 0, \quad (\xi \in \mathbb{R}^n,\ x \in \Omega).$$

is a necessary condition whenever u is a smooth minimizer. This suggests that it is reasonable to assume L is convex in its first argument. In fact, we have the following theorem.

Theorem 1. *Assume L is smooth, bounded below and that the mapping*

$$p \mapsto L(p, z, x)$$

is convex for each $z \in \mathbb{R},\ x \in \Omega$. Then, I is weak lower semicontinuous on $W^{1,q}(\Omega)$.

Proof. Choose any sequence $\{u_k\}_{k=1}^{\infty}$ with $u_k \rightharpoonup u$ in $W^{1,q}(\Omega)$, and set $\ell := \liminf_{k\to\infty} I[u_k]$. We must show $I[u] \leq \ell$. Every weakly convergent sequence is bounded so $\sup_k \|u_k\|_{W^{1,q}(\Omega)} < \infty$.

Upon passing to a subsequence if necessary, suppose also that $\ell = \lim_{k\to\infty} I[u_k]$. Furthermore, $u_k \to u$ strongly in $L^q(\Omega)$. Thus, passing to yet another subsequence if necessary, we have $u_k \to u$ a.e. in Ω.

Fix $\epsilon > 0$. Then the pointwise convergence and Egoroff's Theorem assert

$$u_k \to u \quad \text{uniformly on } E_\epsilon,$$

where E_ϵ is a measurable set with $|\Omega - E_\epsilon| \leq \epsilon$. Let

$$F_\epsilon = \left\{ x \in \Omega : |u(x)| + |\nabla u(x)| \leq \frac{1}{\epsilon} \right\}.$$

Then, $|\Omega - F_\epsilon| \to 0$ as $\epsilon \to 0$. Set $G_\epsilon = E_\epsilon \cap F_\epsilon$ and observe that $|\Omega - G_\epsilon| \to 0$ as $\epsilon \to 0$.

Now, since L is bounded below, we can assume $L \geq 0$ (which is only a shift by some constant). Consequently,

$$\begin{aligned} I[u_k] &= \int_\Omega L(\nabla u_k, u_k, x)\, dx \geq \int_{G_\epsilon} L(\nabla u_k, u_k, x)\, dx \\ &\geq \int_{G_\epsilon} L(\nabla u, u_k, x)\, dx + \int_{G_\epsilon} \partial_p L(\nabla u, u_k, x) \cdot (\nabla u_k - \nabla u)\, dx, \end{aligned}$$

where the last inequality followed from the convexity of L in its first argument. Now, in view of the

definitions of $E_\epsilon, F_\epsilon, G_\epsilon$,

$$\lim_{k\to\infty} \int_{G_\epsilon} L(\nabla u, u_k, x)\, dx = \int_{G_\epsilon} L(\nabla u, u, x)\, dx.$$

In addition, since $\partial_p L(\nabla u, u_k, x) \to \partial_p L(\nabla u, u, x)$ uniformly on G_ϵ and $\nabla u_k \rightharpoonup \nabla u$ in $L^q(\Omega)$, we have

$$\lim_{k\to\infty} \int_{G_\epsilon} \partial_p L(\nabla u, u_k, x) \cdot (\nabla u_k - \nabla u)\, dx = 0.$$

We can deduce that

$$\ell = \lim_{k\to\infty} I[u_k] \geq \int_{G_\epsilon} L(\nabla u, u, x)\, dx,$$

for each $\epsilon > 0$. Recall that $L \geq 0$ and the Monotone Convergence Theorem to conclude

$$\ell \geq \int_\Omega L(\nabla u, u, x)\, dx = I[u],$$

as required. □

Note that the convergence of u_k to u in L^q is much stronger, so we do not need a convexity assumption for $z \mapsto L(p, z, x)$.

We can now establish that I has a minimizer among functions in the admissible set $\mathcal{A}$.

Theorem 2. *Assume L satisfies the coercivity inequality* (1) *and is convex in the variable p. Suppose also that the set $\mathcal{A}$ is nonempty. Then there exists at least one function $u \in \mathcal{A}$ solving*

$$I[u] = \min_{w\in\mathcal{A}} I[w].$$

Proof. Set $m = \inf_{w\in\mathcal{A}} I[w]$. If $m = \infty$ we are done, so assume m is finite. Select a minimizing sequence $\{u_k\}_{k=1}^\infty$. Then $I[u_k] \to m$. Shift L so that $L \geq \alpha|p|^q$ in (1) so that

$$I[w] \geq \alpha \int_\Omega |\nabla w|^q dx.$$

Since m is finite, we conclude that $\sup_k \|\nabla u_k\|_{L^q(\Omega)} < \infty$.

Now fix any function $w \in \mathcal{A}$. Since u_k and w both equal g on $\partial\Omega$ in the trace sense, we have

$u_k - w \in W_0^{1,q}(\Omega)$. Therefore, Poincaré's inequality implies

$$\begin{aligned}\|u_k\|_{L^q(\Omega)} &\leq \|u_k - w\|_{L^q(\Omega)} + \|w\|_{L^q(\Omega)} \\ &\leq C\|\nabla u_k - \nabla w\|_{L^q(\Omega)} + C \leq C,\end{aligned}$$

since $\sup_k \|\nabla u_k\|_{L^q(\Omega)} < \infty$. Hence $\sup_k \|u_k\|_{L^q(\Omega)} < \infty$. These estimates imply $\{u_k\}_{k=1}^{\infty}$ is bounded in $W^{1,q}(\Omega)$.

Consequently, there exists a subsequence $\{u_{k_j}\}_{j=1}^{\infty} \subset \{u_k\}_{k=1}^{\infty}$ and a function $u \in W^{1,q}(\Omega)$ such that $u_{k_j} \rightharpoonup u$ in $W^{1,q}(\Omega)$.

To see that $u \in \mathcal{A}$, note that for $w \in \mathcal{A}$ as above, $u_k - w \in W_0^{1,q}(\Omega)$, which is a weakly closed subspace of $W^{1,q}(\Omega)$. Hence, $u - w \in W_0^{1,q}(\Omega)$. Thus, the trace of u on $\partial\Omega$ is g. Then, $I[u] \leq \liminf_{j\to\infty} I[u_{k_j}] = m$. But since $u \in \mathcal{A}$, it follows that

$$I[u] = m = \min_{w\in\mathcal{A}} I[w].$$

□

There are some mathematically and physically interesting systems that are not covered by the vector version of Theorem 2, which include problems where the Lagrangian $L(P, z, x)$ is not convex in P, but where I is nonetheless weak lower semicontinuous. We use another notion of convexity to study these problems.

Definition 3. *A Lagrangian L is called polyconvex if L has the form*

$$L(P, \mathbf{z}, \mathbf{x}) = F(P, \det P, \mathbf{z}, \mathbf{x}), \quad P \in M^{n\times n}, \quad \mathbf{z} \in \mathbb{R}^n, \quad \mathbf{x} \in \Omega$$

and for each fixed $\mathbf{z}$, $\mathbf{x}$, the joint mapping $(P, r) \mapsto F(P, r, \mathbf{z}, \mathbf{x})$ is convex.

We then use analogous results to Theorems 1 and 2 for weak lower semicontinuity and the existence of minimizers.

Theorem 3. *Suppose $n < q < \infty$ and that L is bounded below and is polyconvex. Then I is weak lower semicontinuous on $W^{1,q}(\Omega; \mathbb{R}^n)$.*

Theorem 4. *Assume $n < q < \infty$ and that L satisfies the coercivity inequality analogous to* (1) *and is polyconvex. Suppose also that the set $\mathcal{A}$ is nonempty. Then there exists $\mathbf{u} \in \mathcal{A}$ solving*

$$I[\mathbf{u}] = \min_{\mathbf{w}\in\mathcal{A}} I[\mathbf{w}].$$

A detailed description of this type of theorem can be found in [4, §7].

Key examples of systems that are polyconvex, but not convex, come from problems in elasticity. In elasticity, where $P(\mathbf{x})$ is the deformation gradient at a point $\mathbf{x}$ in Ω, the components of P reflect local changes under the deformation in the length of curves going through $\mathbf{x}$, the components of $\operatorname{cof} P$ reflect changes in the areas of variously oriented surfaces, and $\det P$ reflects the local change in volume [54].

2.2 Liquid Crystals & Liquid Crystal Models

Liquid crystals are intermediate states of matter, which flow like incompressible viscous fluids but maintain certain optical properties found in crystals [63, p. 3]. The most commonly known liquid crystals consist of rigid, rod-like molecules that tend to align along a preferred direction. In addition to directional ordering, liquid crystal molecules may also present partial positional ordering of their centers of mass. At high temperatures, liquid crystals are found in the isotropic state, with randomly aligned molecules, and behave like ordinary liquids. Upon lowering the temperature, a transition to the nematic phase occurs at a critical temperature, with molecules acquiring orientational order. Upon reaching a lower temperature threshold, liquid crystals may enter the smectic phase and the molecules will develop partial ordering of their centers of mass, that appear to be arranged in a one-dimensional lattice. Furthermore, specifically in the smectic A phase, the molecules tend to be locally perpendicular to the layers.

As described in the introduction, chromonic liquid crystals are lyotropic systems consisting of disk-like molecules that undergo phase transitions from isotropic to nematic, then reaching the hexagonal columnar phase as the concentration of molecules increases. Since a goal of this dissertation is to exploit the chromonic properties of DNA packing in viruses, a good understanding of the different aspects of liquid crystal modeling is very relevant.

Nematic Liquid Crystals

One of the earliest theories to model nematic liquid crystals is the director theory, first proposed by Oseen and Zocher [48], and later reformulated to its present form by Frank [17]. In this approach, the average orientation of molecules at a point in a domain with a unit vector field called the director. Equilibrium states of a liquid crystal occupying a domain $\Omega \subset \mathbb{R}^3$ correspond to energy minimizing states of the Oseen-Frank energy. This is an energy density consisting of quadratic combinations of

the components of $\nabla \mathbf{n}$ and is defined as

$$E_{OF}(\mathbf{n}) = \int_{\Omega} W_{OF}(\mathbf{n}, \nabla \mathbf{n})\, d\mathbf{x}, \tag{4}$$

$$\begin{aligned} W_{OF}(\mathbf{n}, \nabla \mathbf{n}) = {} & K_1(\nabla \cdot \mathbf{n})^2 + K_2(\mathbf{n} \cdot (\nabla \times \mathbf{n}))^2 + K_3|\mathbf{n} \times (\nabla \times \mathbf{n})|^2 \\ & + (K_2 + K_4)\left[\mathrm{tr}(\nabla \mathbf{n})^2 - (\nabla \cdot \mathbf{n})^2\right]. \end{aligned} \tag{5}$$

The terms corresponding to the positive constants K_1, K_2, and K_3 represent the splay, twist, and bend energy densities, respectively. The constants K_1, K_2, K_3, K_4 are generally assumed to satisfy the Ericksen inequalities

$$K_1 > 0, \quad K_2 > 0, \quad K_3 > 0, \quad K_2 \geq |K_4|, \quad 2K_1 \geq K_2 + K_4, \tag{6}$$

which guarantee the coercivity of W_{OF}, that is,

$$W_{OF}(\mathbf{n}, \nabla \mathbf{n}) \geq K|\nabla \mathbf{n}|^2, \mathbf{n} \in S^2.$$

Moreover, this energy density is frame indifferent and indifferent with respect to interchanging $\mathbf{n}$ with $-\mathbf{n}$ (due to the fact that $\mathbf{n}$ is representing molecules that do not differentiate their head from tail).

Throughout this work, it will be assumed that $K_4 = -K_2$ so that the $K_2 + K_4$ term of (5) does not appear. This assumption is often used and makes sense for the analysis in the following sections due to the fact that the $(K_2 + K_4)$ term is what is known as a null Lagrangian; it does not appear in the Euler-Lagrange equations for (4) and lemma 1 confirms that it only depends on the boundary condition.

Defects in the Oseen-Frank theory correspond to points, lines, or surfaces in the liquid crystal domain where $\mathbf{n} = \mathbf{0}$. The energy may become unbounded even at point defects, due to the localization of very high values of $|\nabla \mathbf{n}|$ as the unit vector $\mathbf{n}$ transitions to zero. This is indeed the case of defects in two-dimensional geometries. The order tensor theory of Landau and de Gennes and that of Ericksen of liquid crystals with variable degree of orientation aim at regularizing singular behaviors.

Smectic A Liquid Crystals

Upon lowering the temperature, nematic liquid crystals experience a transition to the smectic A phase, characterized by the one-dimensional ordering of the molecular centers of mass, now located in an array of equally spaced layers. The orientational order of the nematic phase persists, with molecules being aligned along the direction perpendicular to the layers.

When modeling the smectic liquid crystal phase, one must also include an energy term that penalizes departure of the layer locations from their preferred equally-spaced state. In order to describe layer configurations with variable geometry, McMillan [42], together with work by de Gennes, introduced what is called the complex order parameter that carries information on spatial frequency, geometry, and layer density of the smectic phase. This parameter has the form

$$\varphi = \rho(\mathbf{x})e^{i\omega(\mathbf{x})}, \tag{7}$$

where the scalar field ω, when constant, indicates mid-layer locations. The function ρ corresponds to the intensity of the layering, and when $\rho \equiv 0$, the liquid crystal reduces to a nematic phase, with no positional order of the centers of mass of the molecules. When $\rho \equiv 1$, the material has perfect smectic layering.

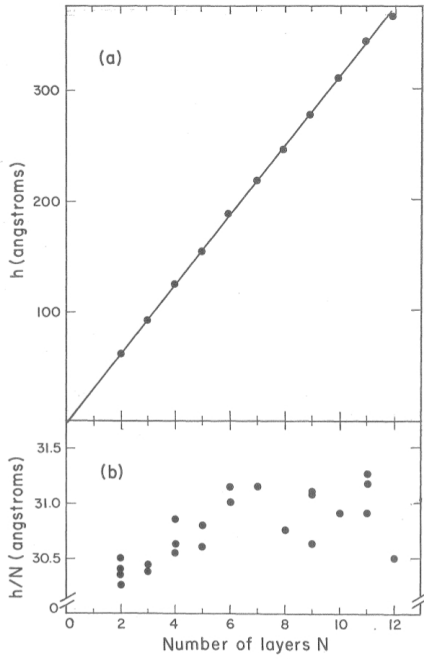

Figure 4: Optical measurements of smectic A layer spacing, from [56]

De Gennes proposed the following model for smectic A liquid crystals with the unit vector field $\mathbf{m}$ representing the director field, and ρ and ω from (7)

$$E_{sm}(\omega, \rho, \mathbf{m}) = E_{OF}(\mathbf{m}) + B_0 \int_\Omega \rho^2 |\nabla\omega - q\mathbf{m}|^2 + |\nabla\rho|^2 d\mathbf{x}, \tag{8}$$

where B_0 is the layer compressibility modulus of the material. Formally, at the limit $B_0 \gg K_1, K_2, K_3$, the constraint $\nabla\omega = q\mathbf{m}$ is satisfied, so that the director field is perpendicular to the level surfaces of ω. The analysis of this model, and particular the phase transitions that it predicts, show a remarkable

agreement with experimental observation [5].

2.3 Results for the Oseen-Frank Energy Functional

Here we follow the roadmap laid out in section 2.1 to show the existence of minimizers for the Oseen-Frank energy from (4).

For a given Lipschitz function $\mathbf{n}_0$, we search for minimizers of (5) in the admissible set

$$\mathcal{A} := \{\mathbf{u} \in H^1(\Omega; \mathbb{R}^3) \ : \ |\mathbf{u}| = 1, \ \text{trace}(\mathbf{u}) = \mathbf{n}_0\}. \tag{9}$$

First, a lemma regarding the $K_2 + K_4$ term.

Lemma 1. *For any Lipschitz function $\mathbf{n}_0 : \partial\Omega \to \mathbb{S}^2$, there is a number $\ell(\mathbf{n}_0)$ such that*

$$\ell(\mathbf{n}_0) = \int_\Omega \left[\text{tr}(\nabla \mathbf{u})^2 - (\nabla \cdot \mathbf{u})^2\right] \ d\mathbf{x},$$

for all $\mathbf{u} \in \mathcal{A}$.

The proof of this is somewhat technical for arbitrary $\mathbf{u} \in \mathcal{A}$, but comes down the fact that

$$\text{tr}(\nabla \mathbf{u})^2 - (\nabla \cdot \mathbf{u})^2 = \nabla \cdot ((\nabla \mathbf{u})\mathbf{u} - (\nabla \cdot \mathbf{u})\mathbf{u})$$

when $|\mathbf{u}| = 1$, and by the divergence theorem, we can write the stated integral as an integral on the boundary, thus depending only on $\mathbf{n}_0$.

For a given choice of positive $K_1, \ K_2, \ K_3$, let

$$\alpha = \min\{K_1, \ K_2, \ K_3\}, \qquad \beta = 3(K_1 + K_2 + K_3),$$

and let

$$\begin{aligned} \tilde{E}_{OF}(\mathbf{u}) &= \int_\Omega \tilde{W}_{OF}(\mathbf{u}, \nabla \mathbf{u}), \\ \tilde{W}_{OF}(\mathbf{u}, \nabla \mathbf{u}) &:= W_{OF}(\mathbf{u}, \nabla \mathbf{u}) + (\alpha - K_2 - K_4)\left[\text{tr}(\nabla \mathbf{u})^2 - (\nabla \cdot \mathbf{u})^2\right] \end{aligned}$$

We can see that $\mathbf{n} \in \mathcal{A}$ is a minimizer for E_{OF} if and only if $\mathbf{n} \in \mathcal{A}$ is a minimizer for $\tilde{E}_{OF}$ since

for any $\mathbf{u} \in \mathcal{A}$,

$$\begin{aligned}\tilde{E}_{OF}(\mathbf{u}) - \tilde{E}_{OF}(\mathbf{n}) &= E_{OF}(\mathbf{u}) + (\alpha - K_2 - K_4)\ell(\mathbf{n}_0) - [E_{OF}(\mathbf{n}) - (\alpha - K_2 - K_4)\ell(\mathbf{n}_0)] \\ &= E_{OF}(\mathbf{u}) - E_{OF}(\mathbf{n}). \end{aligned} \tag{10}$$

Therefore, we now consider the existence of minimizer of the functional $\tilde{E}_{OF}$ in $\mathcal{A}$.

Lemma 2. *The Lagrangian $\tilde{W}_{OF}$ is coercive and bounded for each $\mathbf{u} \in H^1(\Omega; \mathbb{S}^2)$.*

Proof. For $\mathbf{u} \in H^1(\Omega; \mathbb{S}^2)$, we have the following identities

$$\begin{aligned}|\nabla \mathbf{u}|^2 &= \operatorname{tr}(\nabla \mathbf{u})^2 + |\nabla \times \mathbf{u}|^2, \\ |\nabla \times \mathbf{u}|^2 &= (\mathbf{u} \cdot \nabla \times \mathbf{u})^2 + |\mathbf{u} \times \nabla \times \mathbf{u}|^2. \end{aligned} \tag{11}$$

Using these identities and the above definitions of α and β, we have

$$\begin{aligned}\alpha|\nabla \mathbf{u}|^2 &\le \tilde{W}_{OF}(\mathbf{u}, \nabla \mathbf{u}) \\ &= (K_1 - \alpha)(\nabla \cdot \mathbf{u})^2 + K_2(\mathbf{u} \cdot \nabla \times \mathbf{u})^2 + K_3|\mathbf{u} \times \nabla \times \mathbf{u}|^2 + \alpha \operatorname{tr}(\nabla \mathbf{u})^2 \\ &\le 2\beta|\nabla \mathbf{u}|^2. \end{aligned}$$

□

Lemma 3. *$\tilde{W}_{OF}$ is weak lower semicontinuous on $\mathcal{A}$.*

Proof. Theorem 1 implies that we only need to show that $\tilde{W}_{OF}(\mathbf{u}, \nabla \mathbf{u})$ is convex with respect to $\nabla \mathbf{u}$.

Letting $\gamma = \min\{K_2, K_3\}$ and using the identities in (11), we can write

$$\begin{aligned}\tilde{W}_{OF}(\mathbf{u}, \nabla \mathbf{u}) = (K_1 - \alpha)(\nabla \cdot \mathbf{u})^2 + (\gamma - \alpha)|\nabla \times \mathbf{u}|^2 + (K_2 - \gamma)(\mathbf{u} \cdot \nabla \times \mathbf{u})^2 + \\ (K_3 - \gamma)|\mathbf{u} \times \nabla \times \mathbf{u}|^2 + \alpha|\nabla \mathbf{u}|^2.\end{aligned}$$

Since each term is quadratic in $\nabla \mathbf{u}$ and has a nonnegative coefficient, we can conclude $\tilde{W}_{OF}$ is convex with respect to that argument. Thus, $\tilde{W}_{OF}$ is weak lower semicontinuous.

□

Theorem 5. *For any Lipschitz function $\mathbf{n}_0 : \partial\Omega \to \mathbb{S}^2$, there exists an $\mathbf{n} \in \mathcal{A}$ such that*

$$E_{OF}(\mathbf{n}) = \min_{\mathbf{u} \in \mathcal{A}} E_{OF}(\mathbf{u}).$$

Proof. Let $\{\mathbf{n}_k\}$ be a minimizing sequence in $\mathcal{A}$ for the functional $\tilde{E}_{OF}$. This sequence is bounded in H^1 since, for a fixed $\mathbf{w} \in \mathcal{A}$, we know $\mathbf{n}_k - \mathbf{w} \in H_0^1(\Omega;\mathbb{R}^3)$ and so

$$\begin{aligned}\|\mathbf{n}_k\|_{H^1} &\leq \|\mathbf{n}_k - \mathbf{w}\|_{H^1} + \|\mathbf{w}\|_{H^1} \\ &\leq C\|\nabla \mathbf{n}_k - \nabla \mathbf{w}\|_{L^2} + C \\ &\leq C.\end{aligned}$$

Therefore, there exists a subsequence $\{\mathbf{n}_{k_j}\} \subseteq \{\mathbf{n}_k\}$ that weakly converges to a limit $\mathbf{n} \in H^1(\Omega;\mathbb{R}^3)$. Being that $H_0^1(\Omega;\mathbb{R}^3)$ is a closed subspace of $H^1(\Omega;\mathbb{R}^3)$, $\mathbf{n} - \mathbf{w}$ is in $H_0^1(\Omega;\mathbb{R}^3)$ so trace$(\mathbf{n}) = \mathbf{n}_0$. By the compact embedding of H^1 in L^2, it is also true that $\mathbf{n}_{k_j} \to \mathbf{n}$ in L^2. Thus,

$$\|\mathbf{n}_{k_j}\|_{L^2} - \|\mathbf{n}\|_{L^2} \leq \big|\|\mathbf{n}_{k_j}\|_{L^2} - \|\mathbf{n}\|_{L^2}\big| \leq \|\mathbf{n}_{k_j} - \mathbf{n}\|_{L^2} \to 0,$$

and so $|\mathbf{n}| = 1$. Thus, $\mathbf{n} \in \mathcal{A}$. Therefore,

$$\tilde{E}_{OF}(\mathbf{n}) = \min_{\mathbf{u}\in\mathcal{A}} \tilde{E}_{OF}(\mathbf{u}),$$

and from the argument in (10), the result follows. □

Here we also include a theorem from [23] on the regularity of minimizers of the Oseen-Frank energy functional with Lipschitz boundary data.

Theorem 6. *If* $\mathbf{n}$ *in* $H^1(\Omega;\mathbb{R}^3)$ *is a minimizer of* E_{OF}*, then* $\mathbf{n}$ *is analytic on* $\Omega \setminus Z$ *for some relatively closed subset* Z *of* Ω *that has one-dimensional Hausdorff measure zero.*

This regularity result will prove to be essential in using liquid crystal theory to determine the configuration of the DNA filament in bacteriophage capsids. The set of discrete points Z in which $\mathbf{n}$ is not analytic will contain the locations at which the filament spirals to another layer in the spooling, as described in 4.3.

3 Lyotropic Chromonic Liquid Crystals (LCLCs)

The chromonic denomination of this class of liquid crystals emerges directly from the discovery that clustered DNA, in free solution and *in vivo*, may form liquid crystal phases. The PhD dissertation by François Livolant, as well as their other works from around that time, offer the first systematic classification and identification of the liquid crystalline phases of DNA [37, 38, 39].

As mentioned in the introduction and in §2.2, chromonic liquid crystals are made up of plank-like molecules that stack to form columns. By adding these molecules to water, liquid crystal phases form as their concentration changes. First, at very low concentrations, they form small columnar stacks that are randomly oriented. By increasing the concentration, larger columnar units emerge with their axes tending to align along a preferred direction, forming a nematic phase. The nematic director $\mathbf{n}$ of the Oseen-Frank theory is now the average direction of columnar alignment. With further increase of concentration, the columnar units aggregate into groups of six, resulting in a hexagonal crystalline phase on planes transverse to the axis. In what follows, we denote the unit lattice vectors by $\mathbf{m}$ and $\mathbf{p}$ so that the set $\{\mathbf{n}, \mathbf{m}, \mathbf{p}\}$ forms an orthogonal system.

The prototypical model for columnar LCLCs was developed in works by de Gennes and Kléman [21, 29]. The free energy they proposed consists of a sum of a term penalizing distortions of the liquid crystal configuration and of an elastic energy term associated with deformations of the lattice structure. Rather than adding an elastic energy term, the basic model in this section takes the lattice structure as fixed and accounts for its presence with pointwise constraints, discussed below.

We construct a model of the hexagonal columnar phase of chromonic liquid crystal able to predict aggregates and DNA spooling. Since chromonic liquid crystals are also nematic, we first postulate the Oseen-Frank density (5) that accounts for local changes in the average columnar direction. Background and minimization results for this energy are described in Section 2. Altogether, the proposed energy consists of two terms: the Oseen-Frank energy of the nematic phase subject to constraints and a surface energy contribution penalizing the area of the aggregates.

The role of the constraints is to express the large resistance to splay and twist deformation of the molecules. This results in dominance of the splay and twist constants over the bending one. That is,

$$K_1, K_2 \gg K_3.$$

A physical interpretation of such phenomena, given next, can be found in [30, Ch. 5]. The splay of a liquid crystal is zero whenever dislocations do not occur, that is, the same number of filaments that enter a unit area exit that cross-section. In the case of the hexagonal columnar phase, nonzero splay would allow for deviations from the lattice structure. Twist is prohibited because of its incompatibility with the two-dimensional lattice order in planes perpendicular to the director. Setting $\mathbf{n} \cdot \nabla \times \mathbf{n} \equiv 0$ is a necessary and sufficient condition for the envelopes of the director to be perpendicular to a family of surfaces.

The next important feature that is not found in a typical nematic is the cohesive nature of this material. One way to account for this is through surface tension so that the surface area of the domain geometrically constrains the system. Without this information in the energy, the equilibrium shape of toroidal aggregates would no longer exhibit the shapes seen in experiments. Therefore, we

include a term in the energy to penalize diversions from a cohesive state.

The saddle-splay term of (5), the $K_2 + K_4$ term, will not be considered.

Thus, we begin with the most basic model encompassing the above mentioned features. In a domain Ω, with unit director field $\mathbf{n}$ representing the average orientation of the axes of the columns, we have

$$E_{chr} = \int_\Omega K_3 |\mathbf{n} \times \nabla \times \mathbf{n}|^2 d\mathbf{x} + \sigma \,\mathrm{Area}(\partial\Omega), \tag{12}$$

$$|\mathbf{n}| = 1, \tag{13}$$

$$\nabla \cdot \mathbf{n} = 0 \text{ in } \Omega, \tag{14}$$

$$\mathbf{n} \cdot \nabla \times \mathbf{n} = 0 \text{ in } \Omega, \tag{15}$$

$$\mathbf{n} \cdot \boldsymbol{\nu} = 0 \text{ on } \partial\Omega, \tag{16}$$

$$\mathrm{Vol}(\Omega) = V_0, \quad \text{a constant} \tag{17}$$

where $\boldsymbol{\nu}$ is the unit outward normal vector to Ω. The boundary condition (16) expresses the tendency of columnar structures to organize themselves tangentially to the surface. The constant V_0 represents the total volume of chromonic molecules in the solution.

In this expression, the coefficient K_3 is a physical constant accounting for the mild bending resistance of LCLC systems and the parameter σ represents the cohesive force holding the system together. Factoring out K_3 from the energy, we observe that the single parameter σ/K_3 remains. Minimizing the energy (12) leads to a free boundary problem for the cluster shape and director configuration inside. These will be analyzed in Section 6.

Note that this model does not yet include an elastic energy term for the symmetry features of the hexagonal columnar phase nor the density of the liquid crystal. These features, to be discussed later, are relevant to the study of dsDNA encapsidation.

4 DNA Encapsidation

During the last two decades, the study of DNA encapsidation has attracted the attention of many scientists with the aim of solving the amazing puzzle of how a polymeric filament, with persistence length of the same order of magnitude as the capsid diameter, can actually be packed in such a small region. These packing conditions result in extreme pressures, between 30 and 60 atmospheres, inside the capsid. Models were then developed to predict such large pressures.

The great bulk of the earlier work was prior to the availability of cryogenic imaging techniques that we now have at our disposal. Images provide new data, such as the size of the disordered core region at the center of the capsid and density graphs (as in Figure 6) that give indication of the spacing

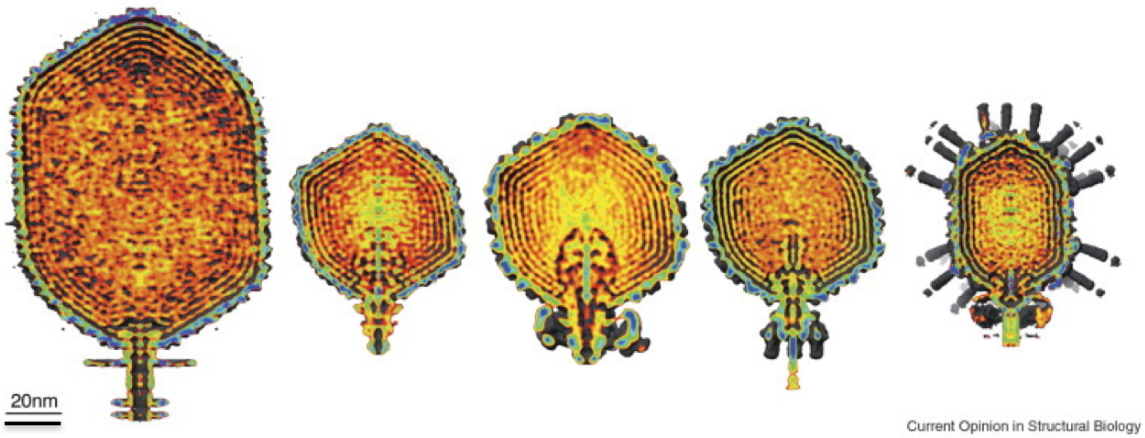

Figure 5: Cryo-EM reconstructions of viruses (left to right) T4, T7, ϵ15, P22, ϕ29 [27]

between adjacent DNA segments. Knowledge of the size of the disordered core provides accurate information on the bending properties of the system and helps towards a better quantification of the parameters of the model, which further aids the design of synthetic viruses.

Now we use a similar strategy to Section 3 to develop a model for the configuration of DNA within bacteriophage capsids. First is a discussion of other modeling approaches that have been used in previous works. Then, we present the model developed in this dissertation as follows:

1. We consider the energy (12) together with the constraints (13) – (16), with the appropriately modified volume relation, given below in (21). We include a bulk energy penalty of the disordered core, whose size is now an unknown of the problem.
2. We include the hexagonal elastic energy of the cross-section to the total energy.
3. We reconstitute the DNA filament and the location of the strands in the capsid.
4. Parameters and their dimensions are discussed.
5. Finally, a potential addition, based on prior work, that accounts for the self-repulsion of the filament are described.

4.1 Prior Models for DNA Packing in Bacteriophages

A large list of authors have worked on modeling DNA configurations in bacteriophages using Monte Carlo and Molecular Dynamics methods, such as [2, 3, 28, 61] to name only a few.

In [2], the authors use a simple molecular mechanics model to investigate the optimal DNA packing configurations in viral capsids. The force constants for the various terms of their energy were

chosen to approximate known physical properties. To account for the confinement imposed by the outer capsid walls, an energy term is included that highly penalizes going outside of the specified bounding radius. The resulting optimal configurations are given in terms of the percentage of the spherical volume is filled by DNA.

Another work applying these types of methods is [28], which focuses on the forces required to package and eject the DNA within a bacteriophage capsid. The energy of a "chain" is calculated as a function of the degree of loading or ejection. They perform Brownian molecular dynamics simulations of DNA loading into a viral capsid, using a coarse-grained model in which the DNA strand is represented by a semi-rigid string of beads. These authors use a cohesive energy, similar to that described below in (19), to account for the hexagonal packing structure and self-repulsion (or -attraction) of the DNA strand. The capsid-particle interactions are described by a short-ranged repulsive potential that vanishes identically for particles within the capsid radius but increases steeply for particles at distances greater than the capsid radius (similar to [2]).

Regarding both of the works described above, we make note of a few things. First is that the hexagonal structure of the packing is either not accounted for or only appears as an assumption in the formulation of the cohesive energy. Also, the energy contribution of the self-repulsion of the DNA strand, among other features, is fit with phenomenological constants. The values may only be valid for a small number of viruses, and thus would need to be reconsidered for each additional virus studied. Lastly, the interaction between the DNA and the capsid walls is not represented in the works above; the authors only enforce the *size* of the capsid, not the protein structures on the walls that are now known to interact the strand.

There are also existing works that have taken a continuum modeling approach to this setting. Now we describe the work [31], which takes a similar approach to ours. As in this paper, they define an elastic energy whose minimizing director field will give the local orientation and density of DNA segments within a virus. The energy is defined as a functional of the director field that accounts for bending, torsion, and for electrostatic interactions through a cohesive energy (also discussed in [28]).

With a variable length director field $\boldsymbol{m}$, where $|\boldsymbol{m}| = u$ gives the local DNA-length density per unit volume, the authors in [31] use rod theory and define the local strain energy per unit volume of DNA due to bending and torsion to be

$$W(\boldsymbol{m}, \nabla\boldsymbol{m}, \nabla\nabla\boldsymbol{m}) = \left\{ \frac{A}{2}\kappa^2 + \frac{B}{2}\tau^2 \right\} |\boldsymbol{m}|, \tag{18}$$

where A and B are, respectively, the bending and torsional stiffnesses, κ is the local curvature, and τ is the local torsion. The vector field $\boldsymbol{m}/|\boldsymbol{m}|$ is equivalent to our director field $\mathbf{n}$.

The authors also assume the DNA has a cohesive energy per unit volume, which is written as a function $\phi(u)$ of the DNA density $u = |\boldsymbol{m}|$. This energy is strongly repulsive at high densities and may be attractive at low densities. They first define what they call the interaction energy per unit length of hexagonally packed DNA, given by

$$e_a(d) = e_0 + \sqrt{3} \int_d^{d_0} \phi_0 \{\exp[-(\xi - d_0)/c] - 1\}\, d\xi,$$

where the following phenomenological values are provided $e_0 = 0.8\ k_B T/\text{nm}$, $\phi_0 = 0.1 k_B T/\text{nm}^3$, $d_0 = 2.8$ nm, and $c = 0.15$ nm. Then the cohesive energy per unit volume is

$$\phi(u) = u e_a(d = \sqrt{(2/\sqrt{3})/u}), \tag{19}$$

the inner expression for d coming from the relationship between spacing and density in hexagonally packed DNA.

4.2 The Free Boundary Model for DNA Encapsidation

We now describe our approach to modeling the packing of DNA within bacteriophage capsids using modeling techniques developed for liquid crystals. As mentioned in the previous section, the proposed model assumes that packed DNA forms chromonic liquid crystal phases. This is a natural assumption especially considering that chromonic liquid crystals are precisely named after DNA structures.

The DNA is treated as a thin elastic filament with embedded rigid units, a feature shared by many biological polymers, giving its packed configuration the well known columnar structure of LCLCs. The notion that DNA segments within capsids form a hexagonal lattice is noted in works such as [33, 61]. The geometry of the capsid and the length of the DNA together induce an orientational order on the rod-like components of the filament, and the tightly-packed spooling will create the effect of layers. This layered structure is clearly exemplified by graphs of the radial density profile within a capsid. See Figure 6, taken from [16], for such a graph. Due to the rigidity of the filament induced by the rods, the DNA is unable to indefinitely spool toward the center of the capsid. Instead, a core region of disorder develops at the center, which will be modeled as an isotropic liquid crystal.

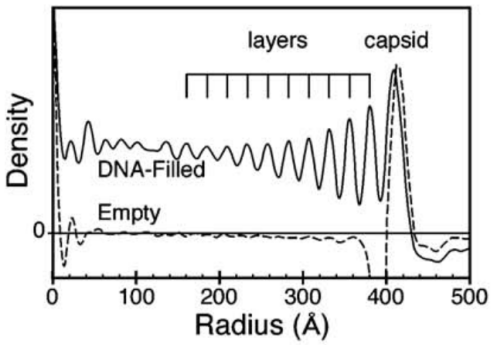

Figure 6: Density profile of the virus T5

Two main mechanisms are at play in determining the packed configurations. One is that the bending resistance of the DNA filament prevents it from filling the entire capsid in an organized manner, and instead becomes disordered when the curvature becomes too large as the filament approaches the center of the capsid. The other main mechanism that contributes to the packing structure is the repulsion between neighboring negatively-charged DNA segments. Indeed, the negative charge of the base pairs, in competition with the bending resistance, determines the resulting packing configuration. Similarly, it is the competition between the bending energy and that of the inner disordered core that determines the radius of the latter.

Another feature of the columnar phase is the lattice in the two-dimensional cross-sections perpendicular to the DNA segments, represented by two unit vectors $\mathbf{m}$ and $\mathbf{p}$. As the strands present resistance to bending, the deformation of the lattice increases the compression and shearing energy of the system. We need to account for all such effects in the energy. This effectively accounts for the self-repulsion of the DNA segments.

In our formulation, we suppose that $\mathbf{n}$ gives the orientation of the embedded rigid rods in the DNA filament and is tangent almost everywhere to a curve, except at a discrete set of defects, where the curve will spiral from one layer to another. This curve will represent the DNA filament. Because $\mathbf{n}$ is tangent to a curve almost everywhere, it is the case that $\nabla \cdot \mathbf{n} \equiv 0$. Also, we will assume that there is no twist in the system for the same reason as with the chromonic model, which was due to the lattice structure perpendicular to the director, and will again set that to zero as a constraint. Thus, we first consider a similar energy to (12), in this case with the exterior boundary being fixed and the interior boundary, dividing the ordered and disordered states, being unknown. An additional term is included that accounts for the energy within the disordered region, which is proportional to the volume of that region.

Suppose $\mathcal{B}$ is the capsid domain and Ω_0 is the isotropic core region. The domain containing the

ordered liquid crystal phase will be defined as $\Omega := \mathcal{B} \setminus \Omega_0$. Then, (12) is modified to

$$E_{cap} = \int_\Omega K_3 |\mathbf{n} \times \nabla \times \mathbf{n}|^2 d\mathbf{x} + \nu \,\mathrm{Vol}(\Omega_0) + \sigma \,\mathrm{Area}(\partial\Omega_0), \tag{20}$$

$$\begin{aligned} &|\mathbf{n}| = 1, \\ &\nabla \cdot \mathbf{n} = 0 \text{ in } \Omega, \\ &\mathbf{n} \cdot \nabla \times \mathbf{n} = 0 \text{ in } \Omega, \\ &\mathbf{n} \cdot \boldsymbol{\nu} = 0 \text{ on } \partial\Omega, \\ &\mathrm{Vol}(\Omega) + \mathrm{Vol}(\Omega_0) = \mathrm{Vol}(\mathcal{B}). \end{aligned} \tag{21}$$

In addition to the bending constant K_3 and the surface tension coefficient σ, the term involving the parameter ν, taken after the Onsager theory of rigid rods, accounts for the energy of the disordered core.

In order to illustrate the competition between the bending energy and the isotropic one, the former tending to increase the size of Ω and the latter to decrease it, we substitute the constraint (21) directly into the energy to get

$$E_{cap} = K_3 \left\{ \int_\Omega \left(|\mathbf{n} \times \nabla \times \mathbf{n}|^2 - \frac{\nu}{K_3} \right) d\mathbf{x} + \frac{\sigma}{K_3} \,\mathrm{Area}(\partial\Omega_0) + \frac{\nu}{K_3} \,\mathrm{Vol}(\mathcal{B}) \right\}. \tag{22}$$

Note that the last term is a constant, and so does not affect energy minimization. Finally, we include the cross-sectional elastic energy to get

$$\begin{aligned} E_{cap} = K_3 \Bigg\{ \int_\Omega \Bigg(|\mathbf{n} \times \nabla \times \mathbf{n}|^2 + \frac{B}{K_3} |\nabla(\mathbf{m} + \mathbf{p})|^2 + \frac{C}{K_3} |\nabla(\mathbf{m} - \mathbf{p})|^2 - \frac{\nu}{K_3} \Bigg) d\mathbf{x} \\ + \frac{\sigma}{K_3} \,\mathrm{Area}(\partial\Omega_0) + \frac{\nu}{K_3} \,\mathrm{Vol}(\mathcal{B}) \Bigg\}, \end{aligned} \tag{23}$$

with constraints (13)-(16), together with the orthogonality relations

$$\mathbf{m} \cdot \mathbf{p} = 0, \quad \mathbf{m} \cdot \mathbf{n} = 0, \quad \mathbf{n} \cdot \mathbf{p} = 0, \quad |\mathbf{m}| = 1 = |\mathbf{p}|. \tag{24}$$

As stated earlier, B and C represent the three-dimensional bulk and shear moduli of the material. Although precise values of such parameters for dsDNA do not seem to be available in the literature, we appeal to the forms proposed by Kléman and Lavrentovich [30]

$$B = \alpha K_3 \left(\frac{R_c}{d} \right)^2, \quad C = \mu B. \tag{25}$$

The contribution of the cross-sectional elastic energy is then represented by

$$B + C = \delta K_3, \quad \delta := \left(\mu + \alpha \left(\frac{R_c}{d}\right)^2\right) \tag{26}$$

with α between 0.1 and 10 and $\mu = \mathcal{O}(1)$ constant, varying among the viruses under consideration. The quantity δ represents the role of the crystalline structure in the energy since it involves the lattice parameter d. Taking $\mu = \alpha$, and using data from the virus T4, we get

$$\delta = \alpha \left(1 + \left(\frac{R_c}{d}\right)^2\right) = \alpha \left(1 + \left(\frac{40}{2.4}\right)^2\right) = (2.8 \times 10^2)\alpha. \tag{27}$$

In particular,

$$\delta = 2.8 \times 10^3, \quad \text{if } \alpha = 10. \tag{28}$$

Since in most configurations of interest the DNA spools around the axis of the capsid, the previous energy can be further simplified. Indeed, since $\mathbf{p} = \mathbf{e}_z$, then $\nabla \mathbf{p} = \mathbf{0}$. Moreover, from the orthogonality relations, we have that $\mathbf{m} = \mathbf{n} \times \mathbf{p}$, thus $|\nabla \mathbf{m}| = |\nabla \mathbf{n}|$. Using the identity

$$(\mathbf{n} \cdot \nabla \times \mathbf{n})^2 + |\mathbf{n} \times \nabla \times \mathbf{n}|^2 + \mathrm{tr}(\nabla \mathbf{n})^2 = |\nabla \mathbf{n}|^2,$$

the energy function (23) becomes

$$E_{cap} = A\Big\{ \int_\Omega \left(|\mathbf{n} \times \nabla \times \mathbf{n}|^2 + K\left(\mathrm{tr}(\nabla \mathbf{n})^2 + (\mathbf{n} \cdot \nabla \times \mathbf{n})^2\right) - \frac{\nu}{A}\right) d\mathbf{x} + \frac{\sigma}{A}\,\mathrm{Area}(\partial\Omega_0) + \frac{\nu}{A}\,\mathrm{Vol}(\mathcal{B})\Big\}, \tag{29}$$

where

$$A = K_3 + B + C, \quad K = \frac{B + C}{A}. \tag{30}$$

Using the expressions for B and C as in (25), we further obtain

$$A = K_3(1 + \delta), \quad K = \frac{\delta}{1 + \delta}, \tag{31}$$

with δ from (26).

4.3 The DNA Filament

Although solving the above minimization problem provides the alignment of the DNA in the domain, it still lacks information about the location of the DNA filament itself. In this subsection, we

provide those details.

The location of the center curve of the DNA is calculated *a posteriori* using the lattice vectors $\{\mathbf{m}, \mathbf{p}\}$ of the cross-sections perpendicular to $\mathbf{n}$, which provide the directions of packing at a point $\mathbf{x}$ in the domain and also act as a space filling mechanism.

Consider a point $\mathbf{x}$ on the surface $\partial\mathcal{B}$ and the DNA center curve at that point $\mathbf{r}(s) = \mathbf{x}$. Let $\{\mathbf{T} := \mathbf{n}, \mathbf{N}, \mathbf{B}\}$ denote the corresponding set of Frénet-Serret vectors of the curve $\mathbf{r}(\cdot)$ at $\mathbf{x}$, and take $\mathbf{m} = \mathbf{N}$ and $\mathbf{p} = \mathbf{B}$ for each $\mathbf{x}$ in $\partial\mathcal{B}$. The directions of packing on the surface are now associated with $\mathbf{m}$ and $\mathbf{p}$. In keeping with the assumption of a spooling arrangement, we further assume that $\mathbf{p}$ points along the capsid axis and remains constant within the ordered region Ω. In this case, $\mathbf{m} = \mathbf{n} \times \mathbf{p}$.

The fields $\mathbf{m}$ and $\mathbf{p}$ will each have an associated complex order parameter (first described in §2.2 and equation (7)), $e^{i\omega}$ and $e^{i\vartheta}$, respectively, where the scalar fields ω and ϑ are such that

$$\nabla\omega \cdot \mathbf{m} = q, \qquad \nabla\vartheta \cdot \mathbf{p} = q, \tag{32}$$

and q is related to the effective diameter of the DNA d by the relation $q = 2\pi/d$. The scalar fields will be used to characterize the spooling of the DNA strand by providing an ordering to the layering of the molecules. To facilitate the description of the configuration, we assume that the capsid and the layer surfaces are axisymmetric with non-intersecting layers of the same family. The families of layer surfaces $\{S^i_{\mathbf{m}}\}_{i=1}^M$ and $\{S^j_{\mathbf{p}}\}_{j=1}^P$, are given by

$$\begin{aligned} \omega(\mathbf{x}) &= m_i, \quad i = 1, \ldots, M, \\ \vartheta(\mathbf{x}) &= p_j, \quad j = 1, \ldots, P, \end{aligned}$$

respectively, where the integers M and P are determined by information about the capsid and DNA strand. A collection of curves that are defined by the intersections of these families of surfaces would be pieced together to represent the DNA filament. The pieces of the curve would be

$$\mathcal{C}_{i,j} = S^i_{\mathbf{m}} \cap S^j_{\mathbf{p}},$$

and the full curve will be found by solving the differential equations

$$\begin{aligned} \mathbf{r}'(s) &= \mathbf{n}(\mathbf{r}(s)), \quad s \in (0, l_{ij}) \\ \mathbf{r}(0) &= \mathbf{r}_0, \end{aligned} \tag{33}$$

where $\mathbf{r}_0$ is the end of the DNA filament and l_{ij} is the length of the segment $\mathcal{C}_{i,j}$.

The regularity result for $\mathbf{n}$, as stated in Theorem 6, becomes important at this point. The discrete

set of points at which $\mathbf{n}$ is not analytic are points called defects. It is at these defects that the DNA filament will jump from one $\mathcal{C}_{i,j}$ to an adjacent $C_{i+1,j}$ or $C_{i,j+1}$.

4.4 Parameters and Dimensions

Here we list the physical parameters of the system, which include the capsid radius, and the persistence length, effective diameter, and length density m_0 of the DNA.

Name	Value	Units
DNA Persistence Length L_p	50×10^{-9} to 55×10^{-9}	m
DNA Diameter d	2×10^{-9}	m
Capsid Radius R_c	40×10^{-9}	m
Capsid height h	38×10^{-9}	m
Boltzmann constant K_B	1.3806×10^{-23}	J/K
room temperature T	298.15	K
atmosphere (atm)	101325	Pa = J/m^3

Table 1: Physical constants used in calculations for DNA spooling in bacteriophages

The DNA cross-sectional length density m_0 is estimated by taking the ratio of the length of a DNA strand to the volume of the container in which it is packed. It has dimensions of one over the square of the length. Thus, for a perfectly packed DNA strand (i.e. no empty space in the volume), we have that the maximum value is $m_0 = 1/(\pi(d/2)^2) = 3.183 \times 10^{17}$ m^{-2} for virus T4. More realistically, for a T4 bacteriophage genome, with length 54 μm, and T4 virus head of radius 50 nm, we get 1.0313×10^{17} m^{-2}. In Table 2, we list data from specific viruses.

Virus	L_p (nm)	d (nm)	c	L (nm)	R_c (nm)	r_c/R_c	m_0 (m^{-2})
T4	55.60	2.40	21.37	55047.6	40.00	0.5500	0.550×10^{17}
T5	58.38	2.94	17.85	39423.8	42.00	0.4286	1.693×10^{17}
T7	52.88	2.60	18.17	12932.0	26.05	0.5889	2.212×10^{17}
ϵ15	53.90	2.55	13.98	12846.0	28.37	0.5735	0.574×10^{17}

Table 2: Physical measurements of four different bacteriophages. The symbol L_p denotes the persistence length of a DNA chain of length L, effective diameter d, molar concentration c in a sphere-like capsid of radius R_c with a measured radius r_c of the disordered core. T4 [36, 46]; T5 [16]; T7 [8]; ϵ15 [26].

Following Tzlil et al. [61] and subsequently [31], we take the bending constant K_3 as

$$K_3 = K_B T L_p m_0. \tag{34}$$

This results in the bending energy penalty in the form K_3/r^2 when $\mathbf{n}$ exhibits a planar concentric spooling, and therefore depends on the square of the curvature, as expected.

The estimates for the model parameters can be found in Table 3. Note that α is a dimensionless tuning parameter. The weak anchoring coefficient is chosen large enough to force the boundary conditions on $\mathbf{n}$ to be planar to the boundary of the capsid.

We conclude this section by introducing the relevant dimensionless parameter groups. Let $L_0 > 0$ denote a typical length scale of the problem, such as the capsid radius R_c. We denote

$$\bar{K}_3 = L_p m_0 L_0, \quad \bar{A} = \bar{K}_3 (1+\delta), \quad \bar{\nu} = \frac{\nu}{K_3(1+\delta)} L_0^2, \quad \bar{\sigma} = \frac{\sigma}{K_3(1+\delta)} L_0. \tag{35}$$

With dimensions, $K_3 = \bar{K}_3 K_B T / L_0$. The ν and σ moduli will be discussed in a later section. The inclusion of the cross-sectional energy results in an effective increase of the bending modulus. This suggests that for a stiffer material, ν and σ will be scaled accordingly. This is also justified by dimensional analysis, which becomes apparent in the calculations of the capsid radius. The scaling is

$$\tilde{\nu} = \bar{\nu}(1+\delta), \quad \tilde{\sigma} = \bar{\sigma}(1+\delta).$$

Constant	Formula	Units
K_3	$K_B T L_p m_0$	J/m
B	$K_3 (R_c/d)^2$	J/m
C	αB	J/m
A	$K_3 + B + C$	J/m
K	$(B+C)/A$	J/m
σ	$\beta K_B T/(L_p d)$	J/m^2
ν	$K_B T \nu_0(c)/R_c^3$	J/m^3

Table 3: DNA packing parameters for the free boundary model

4.5 Remarks on Effective Mechanical Models

Let us conclude this section with some remarks on the effective treatment of the repulsive electrostatic energy by the proposed mechanical models and a possible modification.

The encapsidation model in (20) subject to the constraints (13) – (16) and (21) does not account for the electrostatic repulsion between neighboring segments of DNA. This may result in over-predicted values of the pressure within the capsid. In the works [28, 31], a cohesive energy term was included, with its parameters fit to predict measured pressure values. In this dissertation, we propose a different modeling approach that directly appeals to the liquid crystal nature of the packed DNA structures. Modeling tools developed for the smectic A phase of liquid crystals play a main role in this approach.

The previous models mentioned in this work do not account for possible deviations of DNA segments from ideal level curve locations. In order to address such an issue, we modify them to allow for the relaxation of the orthogonality constraints on $\mathbf{m}$ and $\mathbf{p}$. Inspired by the analogous issue in the smectic A phase, we expand our basic model to be

$$\mathbb{E}_3 = E_{cap} + D \int_\Omega \left(|\nabla\omega - q\mathbf{m}|^2 + |\nabla\vartheta - q\mathbf{p}|^2 \right) d\mathbf{x}. \tag{36}$$

The problem now reduces to minimizing this energy with constraints (13) – (16) and (21). The constant D gives a measure of layer compression and could involve a stochastic component to account for potential noise in the packing structure.

5 Solutions in a Capillary

This section was a collaboration with UMN mathematics graduate student Ashley Earls, and was a motivating example for many of the methods applied in later sections of this work.

A prototypical example of an LCLC, often used in experimental studies, is the coloring Sunset Yellow (SSY). In order to understand the influence of certain boundary anchoring and other conditions on confined LCLCs, a variety of experimental and theoretical works, such as [7, 11, 12, 47] described below, have been conducted using SSY confined to coaxial cylinders. A common assumption among the aforementioned references and also this work is planar anchoring on the outer cylinder, which is motivated by the observation that SSY exhibits natural planar anchoring on smooth glass surfaces [45].

In [7, 11, 12, 47], the authors consider coaxial cylinders containing nematic liquid crystal and investigate the minimizers of the Oseen-Frank energy (without the additional surface tension term with coefficient σ in (12)); the first two references using the one-constant approximation where $K := K_1 = K_2 = K_3$ and $K_4 = 0$.

In reference [7], they assume strong anchoring boundary conditions requiring the director to be normal to the boundaries of both the inner and outer cylinder. They find that when the ratio of the inner

cylinder radius to the outer cylinder radius is greater than or equal to $e^{-\pi}$, a planar configuration with the director pointing along radial lines and without a z-component minimizes the one-constant energy. They find that as the ratio of inner to outer radius approaches zero that the minimizer "escapes to the third dimension," (the escaped-twist configuration); in other words, it has a nonzero z-component.

The work [11] looks at both cases of radial and concentric boundary conditions with a strong anchoring on the outer cylindrical boundary and weak anchoring on the inner cylindrical boundary. They assume the one-constant approximation of the Oseen-Frank energy density, and they too seek to characterize minimizing solutions. Their analysis identifies the planar solution and the escaped-twist solution, like in [7], as the two configurations of interest.

The newer work [12] focuses on configurations requiring no core and brings the saddle-splay term, i.e. the $K_2 + K_4$ term, into their analysis. Most notably, they find the escaped-twist solution exists for $K_2 + K_4 > 2K_2$ and that for $K_2 + K_4 < 2K_2$, only the trivial solution where the director aligns with the axis of the cylinder exists.

Here we analyze the one-constant approximation of E_{cyl}, with the additional surface area penalty, and aim to characterize minimizing solutions based on the relative values of the Oseen-Frank constant K and the constant σ. Concentric configurations will be of interest, so the director will be assumed to be tangent to the outer cylinder at that boundary and weak anchoring will be assumed along the inner boundary. In contrast to other sections, the twist and splay constraints are not applied, and thus, the phase we consider is a columnar nematic rather than a hexagonal columnar phase.

We begin along the lines of [7] and find the core radius size over which the planar solution will minimize the energy. Then, the more delicate case of smaller core sizes is investigated, where we show that the minimizing solution will either have no core and be the escaped-twist configuration or will have a core of radius $\exp(-\pi/2)$ and will be the planar solution, depending on the relative values of σ and K.

The Setup

Consider nematic liquid crystal confined between two coaxial cylinders of height h, the larger of radius 1 and the smaller of radius r_c, centered along the z-axis. We think again of the smaller cylinder as the "disordered core" region, containing isotropic liquid crystal.

Define the domain as

$$\begin{aligned}\Omega &:= \{(r,\theta) : r_c \le r \le 1,\ 0 \le \theta \le 2\pi\},\\ \Omega_0 &:= \{(r,\theta) : 0 \le r < r_c,\ 0 \le \theta \le 2\pi\},\\ \mathcal{C} &= \Omega \times [0,h].\end{aligned}$$

Let $\mathbf{n}_0 = \mathbf{e}_\theta$, the cylindrical basis vector.

We look for minimizers of the simplified energy

$$\begin{aligned}E_{cyl} &= \int_{\mathcal{C}} W_{OF}(\mathbf{n}, \nabla\mathbf{n})\, r dr d\theta dz + \sigma\, \mathrm{Area}(\partial\Omega_0)\\ &= \int_{\mathcal{C}} K|\nabla\mathbf{n}|^2\, r dr d\theta dz + 2\pi\sigma r_c h, \end{aligned} \tag{37}$$

such that $\mathbf{n} = \mathbf{n}_0$ on $\partial\mathcal{C}$, and where K and σ are material constants.

First we take advantage of two lemmas from [7].

Lemma 4. *If* $\mathbf{n}$ *is a minimizer for*

$$\int_{\mathcal{C}} K|\nabla\mathbf{n}|^2\, r dr d\theta dz + 2\pi\sigma r_c h$$

in the set $\mathcal{F} = \{\mathbf{n} \in H^1(\mathcal{C};\ S^2) : \mathbf{n}(r,\theta,z) = \mathbf{n}_0(r,\theta)$ *on* $\partial\mathcal{C}\}$*, then* $\mathbf{n}$ *is independent of* z *and is also a minimizer of*

$$\int_{\Omega} K|\nabla\mathbf{n}|^2\, r dr d\theta + 2\pi\sigma r_c \tag{38}$$

in the set $\mathcal{E} = \{\mathbf{n} \in H^1(\Omega;\ S^2) : \mathbf{n}(r,\theta) = \mathbf{n}_0(r,\theta)$ *on* $\partial\Omega\}$.

Lemma 5. *For each* $r_c \in (0,1)$, $\min_{\mathbf{n}\in\mathcal{E}} E_{cyl}(\mathbf{n})$ *is attained at a map in the set*

$$\mathcal{E}_0 = \{\mathbf{n} \in H^1(\Omega;\ S^2) : \mathbf{n}(r,\theta) = c(r)\mathbf{n}_0(r,\theta) + s(r)(0,0,1)\},$$

where $c^2(r) + s^2(r) = 1$ *for all* r.

From these lemmas, we can conclude that the minimizers of (37) are independent of both z and θ.

Now we explore minimizers of (38) for different sizes of the core radius r_c. From lemmas 4 and 5,

we can consider potential minimizers of the form

$$\mathbf{n}(r,\theta) = \cos\varphi(r)\mathbf{e}_\theta + \sin\varphi(r)\mathbf{e}_z, \tag{39}$$

where $\varphi(r) : [r_c, 1] \mapsto [0, \pi/2]$ is a smooth function representing the angle of the molecules from horizontal with boundary conditions

$$\left.\frac{d\varphi}{dr}\right|_{r=r_c} = 0 \text{ and } \varphi(1) = 0.$$

For this parametrization of $\mathbf{n}$, the energy is

$$\frac{E_{cyl}(\mathbf{n})}{2\pi K} = \int_{r_c}^{1} \left[\left(\frac{d\varphi}{dr}\right)^2 + \frac{\cos^2\varphi}{r^2}\right] r\,dr + \frac{\sigma}{K} r_c. \tag{40}$$

Characterizing Minimizers Based on Inner Radius Size

We begin by investigating minimizing configurations when the radius of the inner cylinder is determined and find the size that distinguishes between equilibrium states. The first regime of core size values to explore is the larger values, which the following lemma covers.

Lemma 6. *For each $r_c \in [e^{-\pi/2}, 1)$, $\mathbf{n}_0$ is the unique minimizer of E_{cyl} in the class $\mathcal{E}_0$.*

Proof. We see that $\mathbf{n} = \mathbf{n}_0$ when $\varphi \equiv 0$, so

$$\begin{aligned}\frac{E_{cyl}(\mathbf{n}) - E_{cyl}(\mathbf{n}_0)}{2\pi K} &= \int_{r_c}^{1} \left[r\left(\frac{d\varphi}{dr}\right)^2 - \frac{\sin^2\varphi}{r}\right] dr \\ &= \int_{0}^{-\log r_c} \left[\left(\frac{d\varphi}{dt}\right)^2 - \sin^2\varphi\right] dt \quad \text{for } t = \log r - \log r_c,\end{aligned}$$

and since $\left.\frac{d\varphi}{dt}\right|_{t=0} = 0$, we can define $\tilde{\varphi}$ to be the even reflection of $\varphi(t)$ over $t = 0$. Thus, $\tilde{\varphi}(\log r_c) = 0$ and $\tilde{\varphi}(-\log r_c) = 0$. In other words, $\tilde{\varphi}$ has Dirichlet boundary conditions. Therefore, we have

$$\begin{aligned}\frac{E_{cyl}(\mathbf{n}) - E_{cyl}(\mathbf{n}_0)}{2\pi K} &= \frac{1}{2}\int_{\log r_c}^{-\log r_c} \left[\left(\frac{d\tilde{\varphi}}{dt}\right)^2 - \sin^2\tilde{\varphi}\right] dt \\ &= \frac{1}{2}\int_{\log r_c}^{-\log r_c} \left[\left(\frac{d\tilde{\varphi}}{dt}\right)^2 - \tilde{\varphi}^2 + \tilde{\varphi}^2 - \sin^2\tilde{\varphi}\right] dt \\ &\geq 0\end{aligned}$$

since $\tilde{\varphi}^2 - \sin^2\tilde{\varphi} \geq 0$ and, by the Poincare inequality,

$$\int_{\log r_c}^{-\log r_c} \left(\frac{d\tilde{\varphi}}{dt}\right)^2 dt \geq \left(\frac{\pi}{2|\log r_c|}\right)^2 \int_{\log r_c}^{-\log r_c} \tilde{\varphi}^2 \, dt$$

for $r_c \geq e^{-\pi/2}$. We can also note that for $r_c \geq e^{-\pi/2}$, $(E_{cyl}(\mathbf{n}) - E_{cyl}(\mathbf{n}_0))/(2\pi K) = 0$ if and only if $\varphi \equiv 0$, so $\mathbf{n}_0$ is the unique minimizer. □

Note that if $r_c \in (0, e^{-\pi/2})$, $\mathbf{n}_0$ is not a minimizer for E_{cyl}. As an example, consider the function

$$\varphi(r) = \beta \sin\left(\frac{\pi \log r}{2|\log r_c|}\right).$$

Then the associated $\mathbf{n}$ is such that $E_{cyl}(\mathbf{n}) < E_{cyl}(\mathbf{n}_0)$ for small values of the coefficient β. Thus, we consider this core size regime separately.

To begin to learn about minimizers when the inner radius is smaller than $e^{-\pi/2}$, we find the Euler-Lagrange equations for φ. For fixed $\gamma \in H_0^1((r_c, 1))$, define

$$i(\tau) = 2\pi \int_{r_c}^1 \left[r\left(\frac{d\varphi}{dr} + \tau\frac{d\gamma}{dr}\right)^2 + \frac{\cos^2(\varphi + \tau\gamma)}{r} \right] dr$$

Then

$$\begin{aligned} i'(0) &= 2\pi \int_{r_c}^1 \left[2r\left(\frac{d\varphi}{dr} + \tau\frac{d\gamma}{dr}\right)\frac{d\gamma}{dr} - \frac{2\sin(\varphi+\tau\gamma)\cos(\varphi+\tau\gamma)}{r}\gamma \right]\Bigg|_{\tau=0} dr \\ &= 4\pi \int_{r_c}^1 \left(r\frac{d\varphi}{dr}\frac{d\gamma}{dr} - \frac{\sin\varphi\cos\varphi}{r}\gamma \right) dr \\ &= -4\pi \int_{r_c}^1 \left(\frac{d}{dr}\left(r\frac{d\varphi}{dr}\right) + \frac{\sin\varphi\cos\varphi}{r} \right)\gamma \, dr. \end{aligned}$$

Thus any minimum of E_{cyl} must satisfy

$$\frac{d}{dr}\left(r\frac{d\varphi}{dr}\right) = -\frac{\sin\varphi\cos\varphi}{r}. \tag{41}$$

Integrating once, we get

$$\left(r\frac{d\varphi}{dr}\right)^2 = A^2 - \sin^2\varphi, \tag{42}$$

where A is a constant. Cladis and Kléman found in [11] that the energy when $A > 1$ is always greater than when $A \leq 1$, so we consider only the latter case.

Suppose $A \leq 1$. The solution to (42) in that case is

$$r = \exp\left[-F_e\left(\arcsin\left(\frac{\sin\varphi}{A}\right), A\right)\right],$$

where F_e is the incomplete elliptic integral of the first kind. We solve for φ in the expression above and find

$$\varphi = \arcsin\left[A\,\mathrm{sn}\left(\log\frac{1}{r}, A\right)\right], \tag{43}$$

where sn is a Jacobi elliptic function.

The additional requirement

$$\left.\frac{d\varphi}{dr}\right|_{r=r_c} = 0$$

guarantees that net torque is zero at the core interface. Such a solution exists for $r_c = r_0$, where

$$r_0(A) = \exp(-K_e(A)) = \exp\left(-\int_0^{\pi/2} \frac{1}{\sqrt{1 - A^2\sin^2\theta}}\, d\theta\right),$$

where K_e is the complete elliptic integral of the first kind.

In the special case $A^2 = 1$, the solution is

$$\varphi^* = \arcsin\left(\frac{1 - r^2}{1 + r^2}\right).$$

Note that in this case, $r_0 = 0$. In other words, no core is exhibited when $A = 1$. Also, in the special case $A^2 = 0$, the solution reduces to the previous regime with $\varphi \equiv 0$ and $r_c = r_0(0) = e^{-\pi/2}$.

Now we search for the value of A that gives the lowest energy. The value of A gives both the size of the core needed and the angle φ of the director at all radii r. The following lemma demonstrates that a minimum will fall within one of these special cases.

Lemma 7. *Let $0 < A_* < 1$ be a critical point of the energy. Then there is a local maximum of the energy at that value.*

Proof. Let $E_{cyl}(A)$ denote the energy associated to A. The derivative of E_{cyl} with respect to A is

$$\begin{aligned}\frac{\partial E_{cyl}}{\partial A} &= -\left[r\left(\frac{d\varphi}{dr}\right)^2 + \frac{\cos^2\varphi}{r}\right]\Big|_{r=r_0(A)}\left(\frac{dr_0}{dA}\right) + \frac{\sigma}{K}\left(\frac{dr_0}{dA}\right) \\ &= \left(\frac{\sigma}{K} - \frac{1-A^2}{r_0(A)}\right)\frac{dr_0}{dA}, \end{aligned} \tag{44}$$

with

$$\frac{dr_0}{dA} = -r_0\int_0^{\pi/2} \frac{A\sin^2\theta}{(1-A^2\sin^2\theta)^{3/2}}\,d\theta. \tag{45}$$

This derivative (45) is nonzero when A is nonzero, therefore critical points A in $(0,1)$ must satisfy

$$\left(\frac{\sigma}{K} - \frac{1-A^2}{r_0(A)}\right) = 0. \tag{46}$$

Now we find the second derivative in order to determine whether a critical point is a maximum or minimum. The second derivative of the energy with respect to A is

$$\frac{\partial^2 E_{cyl}}{\partial A^2} = r_0'(A)\left(\frac{2Ar_0(A) + (1-A^2)r_0'(A)}{(r_0(A))^2}\right) + r_0''(A)\left(\frac{\sigma}{K} - \frac{1-A^2}{r_0(A)}\right).$$

Now take A_* to be a critical point of E_{cyl} satisfying (46). Then

$$\left.\frac{\partial^2 E_{cyl}}{\partial A^2}\right|_{A=A_*} = r_0'(A_*)\left(\frac{2A_*r_0(A_*) + (1-A_*^2)r_0'(A_*)}{(r_0(A_*))^2}\right).$$

Being that $r_0(A) \geq 0$ and $r_0'(A) \leq 0$ for all A, to prove the lemma, we need to show

$$2A_*r_0(A_*) + (1-A_*^2)r_0'(A_*) > 0.$$

Let K_e be the complete elliptic integral of the first kind, and let E_e be the complete elliptic integral

of the second kind. Note that $K_e(A) \geq \pi/2$ and $E_e(A) \leq \pi/2$ for all A in $(0,1)$. Then,

$$\begin{aligned}
2Ar_0 + (1-A^2)r_0' &= 2Ar_0 - (1-A^2)r_0 \int_0^{\pi/2} \frac{A\sin^2\theta\, d\theta}{(1-A^2\sin^2\theta)^{3/2}} \\
&= \left(2A + (1-A^2)\frac{(1-A^2)K_e(A) - E_e(A)}{A(1-A^2)}\right) r_0 \\
&\geq \left(2A + \frac{(1-A^2)\pi/2 - \pi/2}{A}\right) r_0 \\
&= \left(2 - \frac{\pi}{2}\right) Ar_0 \\
&> 0.
\end{aligned}$$

Thus, the energy is concave down for all A in $(0,1)$, so every critical point $0 < A_* < 1$ is a maximum. □

Characterizing Minimizers Based on Constants

Now, we can summarize how to characterize the minimizers based on the value σ/K with the following theorem.

Theorem 7. *The energy $E_{cyl}(\mathbf{n})$ is minimized by either the planar concentric solution ($A = 0$) or the escaped twist solution with no core ($A = 1$), depending on the value of the surface energy constant σ/K relative to the threshold value of $c \approx 2.06$.*

Proof. From the previous lemma, we can conclude that the minimum value of the energy E_{cyl} is achieved at either $A = 0$ or $A = 1$. We have that

$$\frac{E_{cyl}(A=1)}{2\pi K} = 2,$$

$$\text{and} \quad \frac{E_{cyl}(A=0)}{2\pi K} = \int_{r_0(0)}^{1} \frac{1}{r}\, dr + \frac{\sigma}{K} r_0(0) = -\log(r_0(0)) + \frac{\sigma}{K} r_0(0) = \frac{\pi}{2} + \frac{\sigma}{K} e^{-\pi/2}$$

Let us define the following constant

$$c := (2 - \pi/2)e^{\pi/2} \approx 2.06.$$

Then for $\sigma/K > c$, the energy with $A = 1$ is less than the energy with $A = 0$, and for $\sigma/K < c$, the energy with $A = 1$ is greater than that with $A = 0$. This is because, if we suppose $\sigma/K > c$,

$$(2 - \pi/2)e^{\pi/2} < \frac{\sigma}{K},$$

which implies that

$$2 < \frac{\pi}{2} + \frac{\sigma}{K} e^{-\pi/2}.$$

Thus we can conclude $E_{cyl}(A = 1) < E_{cyl}(A = 0)$. The other inequality follows from the same argument. □

To provide some perspective on σ/K, first let us discuss dimensions of these parameters. The liquid crystal modulus typically has units of Newtons, and in terms of the dimensionless K, is defined as

$$\bar{K} = \frac{K K_B T}{L_0},$$

where L_0 is a typical length scale, K_B is the Boltzmann constant, and T is the temperature in degrees Kelvin. The constant σ would have had dimensions of "energy per unit area" amounting to

$$\bar{\sigma} = \frac{\sigma K_B T}{L_0^2}.$$

In the well-studied liquid crystals *not* belonging to the chromonic family, meaning it has small rod-like molecules and changes phase with temperature, we can say a bit more about this ratio. A typical value for $\bar{K_3}$ in this type of liquid crystal is $\bar{K_3} = 4.8 \times 10^{-12}$ N [63]. There are molecular dynamics works that have been focused on determining the surface tension per unit area between nematic and isotropic phases, and [15] suggests

$$\bar{\sigma} = \frac{0.257 K_B T}{\bar{L}\bar{d}},$$

where $\bar{L} = 2$ nm is the length of a molecule and $\bar{d} = 0.5$ nm is the diameter of a molecule. Thus,

$$\bar{\sigma} = 0.257(1.4 \times 10^{-3}) T \text{ J/m}^2.$$

The length scale we have used throughout this section is the radius of the cylinder, assuming it to be thin.

6 Solutions in LCLCs

The goal of this section is to demonstrate the applicability of our proposed model for hexagonal columnar LCLCs in geometries of interest. The focus will be on equilibrium shapes, and exploring the outcomes when the relative importance of surface interactions versus the resistance to bending is altered.

6.1 Existence of Solutions in a Fixed Domain

We begin by showing the existence of minimizers of the Oseen-Frank energy (4) with constraints (13) – (16). This amounts to showing that minimizers exist for E_{chr} and E_{cap} in a fixed domain, meaning that no boundaries are free or to be determined, to lay some groundwork for the next sections.

Suppose we are in a domain Ω with Lipschitz boundary $\partial\Omega$. Minimizing these energies amounts to looking for minimizers of the energy with density

$$W_{OF}(\mathbf{n}, \nabla\mathbf{n}) = K_1(\nabla\cdot\mathbf{n})^2 + K_2(\mathbf{n}\cdot(\nabla\times\mathbf{n}))^2 + K_3|\mathbf{n}\times(\nabla\times\mathbf{n})|^2$$

in the admissible set

$$\mathcal{A} = \{\mathbf{n}\in H^1(\Omega;\mathbb{R}^3) \ : \ |\mathbf{n}| = 1,\ \nabla\cdot\mathbf{n} = 0 = \mathbf{n}\cdot\nabla\times\mathbf{n} \text{ in } \Omega,\ \text{trace}(\mathbf{n}) = \mathbf{n}_0\} \tag{47}$$

for a given Lipschitz function $\mathbf{n}_0$. Thus, we prove the existence of minimizers $\mathbf{n}$ of the following problem

$$E_{OF}(\mathbf{n}) = \min_{\mathbf{u}\in\mathcal{A}} E_{OF}(\mathbf{u}).$$

Theorem 8. *Suppose $\Omega\subset\mathbb{R}^3$ is a bounded domain with Lipschitz boundary. Then there exists a minimizer $\mathbf{n}$ of W_{OF} in $\mathcal{A}$ that is analytic at all but a relatively closed subset of Ω of one-dimensional Hausdorff measure zero.*

Furthermore, there exist vector fields $\mathbf{m}$ and $\mathbf{p}$ and scalar fields ω and ϑ such that

i.) $\mathbf{n}\cdot\mathbf{m} = \mathbf{m}\cdot\mathbf{p} = \mathbf{n}\cdot\mathbf{p} = 0$ *almost everywhere in* Ω,

ii.) $\nabla\omega\cdot\mathbf{m} = q,\ \nabla\vartheta\cdot\mathbf{p} = q$ *in* Ω.

Proof. We repeat the part of the proof of Theorem 5 showing that a minimizing sequence $\{\mathbf{n}_k\}\subseteq\mathcal{A}$ converges to a limit $\mathbf{n}\in H^1(\Omega;\mathbb{S}^2)$ such that $|\mathbf{n}| = 1$ and $\text{trace}(\mathbf{n}) = \mathbf{n}_0$:

Let $\{\mathbf{n}_k\}$ be a minimizing sequence in $\mathcal{A}$ for the functional $\tilde{E}_{OF}$. This sequence is bounded in H^1 since, for a fixed $\mathbf{w}\in\mathcal{A}$, we know $\mathbf{n}_k - \mathbf{w}\in H^1_0(\Omega;\mathbb{R}^3)$ and so

$$\begin{aligned}\|\mathbf{n}_k\|_{H^1} &\le \|\mathbf{n}_k - \mathbf{w}\|_{H^1} + \|\mathbf{w}\|_{H^1}\\ &\le C\|\nabla\mathbf{n}_k - \nabla\mathbf{w}\|_{L^2} + C\\ &\le C.\end{aligned}$$

Therefore, there exists a subsequence $\{\mathbf{n}_{k_j}\}\subseteq\{\mathbf{n}_k\}$ that weakly converges to a limit $\mathbf{n}\in H^1(\Omega;\mathbb{R}^3)$.

Being that $H_0^1(\Omega;\mathbb{R}^3)$ is a closed subspace of $H^1(\Omega;\mathbb{R}^3)$, $\mathbf{n}-\mathbf{w}$ is in $H_0^1(\Omega;\mathbb{R}^3)$ so trace$(\mathbf{n}) = \mathbf{n}_0$. By the compact embedding of H^1 in L^2, it is also true that $\mathbf{n}_{k_j} \to \mathbf{n}$ in L^2. Thus,

$$\|\mathbf{n}_{k_j}\|_{L^2} - \|\mathbf{n}\|_{L^2} \leq \left|\|\mathbf{n}_{k_j}\|_{L^2} - \|\mathbf{n}\|_{L^2}\right| \leq \|\mathbf{n}_{k_j} - \mathbf{n}\|_{L^2} \to 0,$$

and so $|\mathbf{n}| = 1$.

To show that the limit $\mathbf{n}$ satisfies the constraints $\nabla \cdot \mathbf{n} = 0$ and $\mathbf{n} \cdot \nabla \times \mathbf{n} = 0$ in Ω, first note that due to the convergence in H^1, $\nabla \mathbf{n}_k \rightharpoonup \nabla \mathbf{n}$ in L^2. Therefore,

$$\begin{aligned}
(\mathbf{n}_k)_{i,j} &\rightharpoonup \mathbf{n}_{i,j} \quad \text{for each } i,j = 1,2,3,\\
\sum_{j=1}^{3} (\mathbf{n}_k)_{j,j} &\rightharpoonup \sum_{j=1}^{3} \mathbf{n}_{j,j},\\
\varepsilon_{ij\ell}(\mathbf{n}_k)_{j,\ell} &\rightharpoonup \varepsilon_{ij\ell}\mathbf{n}_{j,\ell} \quad \text{for each } i,
\end{aligned}$$

so we have

$$\begin{aligned}
\nabla \cdot \mathbf{n}_k &\rightharpoonup \nabla \cdot \mathbf{n},\\
\nabla \times \mathbf{n}_k &\rightharpoonup \nabla \times \mathbf{n} \text{ in } L^2.
\end{aligned}$$

Now note that the inner product of a weakly convergent sequence and strongly convergent sequence in L^2 is weakly convergent in L^1, since for $\mathbf{v}_n \to \mathbf{v}$, $\mathbf{w}_n \rightharpoonup \mathbf{w}$ in $L^2$and $\psi \in L^\infty$,

$$\begin{aligned}
\left|\int (\mathbf{v}_n \cdot \mathbf{w}_n)\psi - \int (\mathbf{v}\cdot\mathbf{w})\psi\right| &= \left|\int (\mathbf{w}_n \cdot (\mathbf{v}_n - \mathbf{v}) + \mathbf{v}\cdot(\mathbf{w}_n - \mathbf{w}))\psi\right|\\
&\leq \|\psi\|_{L^\infty}\|\mathbf{w}_n\|_{L^2}\|\mathbf{v}_n - \mathbf{v}\|_{L^2} + \left|\int (\mathbf{w}_n - \mathbf{w})\cdot\psi\mathbf{v}\right|\\
&\to 0,
\end{aligned}$$

so that $\mathbf{n}_k \cdot \nabla \times \mathbf{n}_k \rightharpoonup \mathbf{n}\cdot\nabla\times\mathbf{n}$ in L^1.

Due to the fact that $\mathbf{n}_k \in \mathcal{A}$, we have that the following are all true

$$\begin{aligned}
\nabla \cdot \mathbf{n}_k \rightharpoonup \nabla\cdot\mathbf{n} \quad \text{and} \quad \nabla\cdot\mathbf{n}_k \rightharpoonup 0 \quad \text{in } L^2,\\
\mathbf{n}_k \cdot \nabla\times\mathbf{n} \rightharpoonup \mathbf{n}\cdot\nabla\times\mathbf{n} \quad \text{and} \quad \mathbf{n}_k\cdot\nabla\times\mathbf{n}_k \rightharpoonup 0 \quad \text{in } L^1,
\end{aligned}$$

and by the uniqueness of limits, we can conclude that there exists a minimizer $\mathbf{n} \in \mathcal{A}$. The regularity result follows directly from Theorem 6.

Because $\mathbf{n}$ is analytic almost everywhere, we can find vectors $\mathbf{m}$ and $\mathbf{p}$ such that *i.* holds; for example, we can define them to be the normal and binormal vectors to the curve to which $\mathbf{n}$ is

almost everywhere tangent. With $\mathbf{m}$ and $\mathbf{p}$ thereafter known, the differential equations in *ii.* can be integrated to find ω and ϑ. □

6.2 Solutions in a Torus with Elliptic Cross-section

The next scenario that we investigate arises when considering the superstructures formed by aggregates of chromonic columns folding on themselves or the toroids formed by DNA filaments under certain conditions. Features of these systems differ, with the stiffness of DNA causing a large resistance to bending and the cohesive nature of LCLCs, which affects the size and shape of the toroids that form in each case. Therefore, we use our model to determine the toroidal shape that forms in the following two scenarios: when bending is the dominant contribution to the energy and when surface interactions dominate.

Suppose $\mathbf{n}$ is the given director of the liquid crystal molecules within one of these clusters Ω. Then the energy we aim to minimize with respect to the domain Ω is given by

$$E_{chr} = \int_{\Omega} K_3 |\mathbf{n} \times \nabla \times \mathbf{n}|^2 \, d\mathbf{x} + \sigma \, \mathrm{Area}(\partial\Omega)$$

along with some assumptions on Ω, discussed later. There are measured values for the constant K_3, and the constant σ will account for the relative importance of the cohesive nature of the substance.

The domain under consideration is a toroidal shape, formed by revolving an elliptic disc about the z-axis. See Figure 7 below. We will define a coordinate system to suit this domain in the following way. Let a and b be the lengths of the semi-major and semi-minor axes, respectively, of the ellipse that has been revolved, and r be the radial distance from the center of the ellipse. Let R be the radius of the circle forming the center of the toroid. Let θ be the planar angle about the torus, and let γ be the angle about the elliptic cross-section.

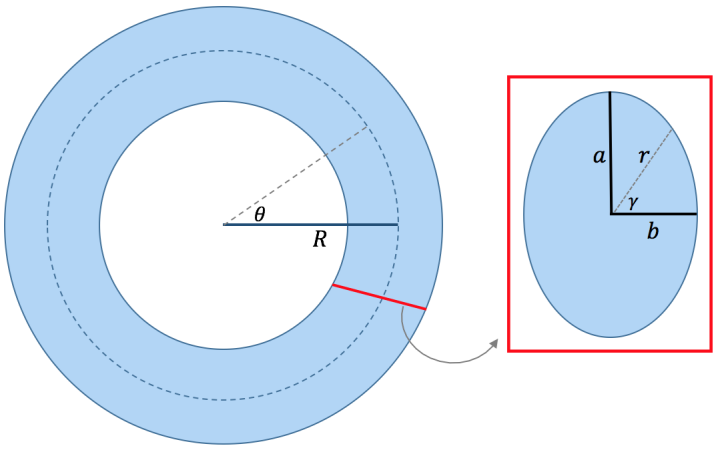

Figure 7: Toroidal domain Ω

Then, if the center line of the torus is laying in the xy-plane, with axis along the z-axis, we have the following relationships

$$\begin{aligned} x &= (R + r\cos\gamma)\cos\theta, \\ y &= (R + r\cos\gamma)\sin\theta, \\ z &= r\sin\gamma. \end{aligned}$$

Now we consider minimizing the energy E_{chr} with respect to the domain Ω. The molecules within a cluster have axes parallel to the central axis of the cluster so, we assume the director $\mathbf{n} = \mathbf{e}_\theta = (-\sin\theta, \cos\theta, 0)$. Then, in these toroidal coordinates,

$$\begin{aligned} \nabla \times \mathbf{e}_\theta &= \frac{1}{R + r\cos\gamma}(\sin\gamma, 0, \cos\gamma), \\ \mathbf{e}_\theta \times (\nabla \times \mathbf{e}_\theta) &= \frac{1}{R + r\cos\gamma}(\cos\gamma, 0, -\sin\gamma), \\ |\mathbf{e}_\theta \times (\nabla \times \mathbf{e}_\theta)|^2 &= \frac{1}{(R + r\cos\gamma)^2}. \end{aligned} \tag{48}$$

The other term in the energy expression is the surface area penalty, which is given by

$$\text{Area}(\partial\Omega) = 4aE_e\left(\sqrt{1 - b^2/a^2}\right)2\pi R, \tag{49}$$

$$\text{with } E_e(k) = \int_0^{\pi/2} \sqrt{1 - k^2\sin^2\vartheta}\, d\vartheta, \tag{50}$$

where $E_e(k)$ is the complete elliptic integral of the second kind.

Therefore the K_3 term, the energy of the twist, is

$$E_{tw} = K_3 \int_\Omega \frac{1}{(R + r\cos\gamma)^2}\, r(R + r\cos\gamma) dr d\gamma d\theta. \tag{51}$$

In order to evaluate this integral to get an expression in terms of the unknown parameters a, b and R, suppose we switch to cylindrical coordinates denoted (ρ, θ, z), with θ the same as above, and let $\mathcal{E}$ be the elliptic cross-section of Ω at $\theta = 0$. We can rewrite the energy above in this coordinate system as

$$E_{tw} = K_3 \int_0^{2\pi} \int_{\mathcal{E}} \frac{1}{\rho^2}\, \rho d\rho dz d\theta \tag{52}$$

Now applying Green's theorem and parametrizing the boundary of $\mathcal{E}$ by $\rho = R + b\cos\gamma$, $z = a\sin\gamma$, and $dz = a\cos\gamma d\gamma$, we have

$$\begin{aligned}
E_{tw} &= K_3 \int_0^{2\pi} \int_{\partial\mathcal{E}} \log(\rho)\, dz d\theta && (53)\\
&= K_3 \int_0^{2\pi} \int_0^{2\pi} \log(R + b\cos\gamma) a\cos\gamma\, d\gamma d\theta && (54)\\
&= K_3 \int_0^{2\pi} a \left[\sin\gamma \log(R + b\cos\gamma)\Big|_0^{2\pi} + \frac{b}{R} \int_0^{2\pi} \frac{\sin^2\gamma}{1 + \frac{b}{R}\cos\gamma} d\gamma \right] d\theta \\
&= K_3 \int_0^{2\pi} \frac{ab}{R} \left[\int_0^{2\pi} \left(\frac{2u}{1+u^2} \right)^2 \frac{2}{(1+u^2) + \frac{b}{R}(1-u^2)} du \right] d\theta, \qquad \text{where } u = \tan(\gamma/2) \\
&= K_3 \int_0^{2\pi} \frac{8ab}{R-b} \left[\int_0^{2\pi} \frac{u^2}{(1+u^2)^2(\alpha^2+u^2)} du \right] d\theta, \qquad \text{with } \alpha^2 = \frac{1 + b/R}{1 - b/R} \\
&= K_3 \int_0^{2\pi} \frac{8ab}{R-b} \left(\frac{\pi}{4(\alpha+1)^2} \right) d\theta \\
&= K_3 \frac{2\pi^2 ab}{R + \sqrt{R^2 - b^2}}. && (55)
\end{aligned}$$

Thus, the full energy in terms of a, b, and R is

$$E_{chr} = K_3 \frac{2\pi^2 ab}{R + \sqrt{R^2 - b^2}} + \sigma \left(8\pi a R E_e \left(\sqrt{1 - b^2/a^2} \right) \right) \tag{56}$$

We consider tori made of a fixed amount of material, meaning that the volume of the domain is constant. We require

$$\mathrm{Vol}(\Omega) = 2\pi^2 abR = V_0. \tag{57}$$

This constraint, along with the requirement that $a \geq b \geq d/2$, where d is the diameter of a molecule, dictates the following constraints on the parameters

$$\begin{aligned} a &= V_0/(2\pi^2 bR), \\ d/2 \leq b &\leq R, \\ b \leq R &\leq 2V_0/(\pi^2 d^2). \end{aligned}$$

Therefore, we can eliminate a and minimize with respect to (b, R) in a compact domain, which we call $\mathcal{S}$.

We now have all of the information needed to find the energy minimizing toroidal shape. The existence of minimizing (b, R) in $\mathcal{S}$ is guaranteed by the Extreme Value Theorem, so all that remains is characterizing minima of E_{chr} with respect to the relative values of K_3 and σ. We will consider each limiting scenario, $K_3 \gg \sigma$ and $\sigma \gg K_3$. Note that for functions f and g, the minima of $f + \epsilon g$ will approach the minima of f as ϵ approaches zero.

Let k be defined so that

$$k^2 := 1 - b^2/a^2 = 1 - \frac{4\pi^4 R^2 b^4}{V_0^2}, \quad \text{using (57).}$$

The following are the components of the gradient of E_{chr} with respect to (b, R)

$$\frac{\partial E_{chr}}{\partial b} = K_3 \frac{V_0 b}{R\sqrt{R^2 - b^2}(R + \sqrt{R^2 - b^2})^2} - \sigma \frac{4V_0}{\pi b^2} E_e(k) - \sigma \frac{32\pi^3 R^2 b^2}{V_0 k^2}(E_e(k) - K_e(k)), \tag{58}$$

$$\frac{\partial E_{chr}}{\partial R} = K_3 \frac{-V_0}{R^2\sqrt{R^2 - b^2}} - \sigma \frac{16\pi^3 R b^3}{V_0 k^2}(E_e(k) - K_e(k)), \tag{59}$$

where K_e is the complete elliptic integral of the first kind and E_e is the complete elliptic integral of the second kind as above.

Minimizing when Bending Dominates

Let us first consider the limiting case where bending costs much more energy than surface interactions with the surrounding medium. Let $\epsilon_b := \sigma/K_3 \ll 1$. Then we aim to minimize

$$E_b := E_{chr}/K_3 = \frac{V_0}{R^2(1 + \sqrt{1 - b^2/R^2})} + \epsilon_b \left(\frac{4V_0}{\pi b} E_e(k) \right), \tag{60}$$

which is the same expression as (56) but the volume constraint in (57) has been used to write a in terms of b and R. Minimizing (60) as $\epsilon_b \to 0$ amounts to minimizing its first term, and by inspecting the K_3 terms of its gradient, one notices

$$\left.\frac{\partial E_b}{\partial b}\right|_{\epsilon_b \to 0} \geq 0, \quad \left.\frac{\partial E_b}{\partial R}\right|_{\epsilon_b \to 0} \leq 0, \quad \text{for all } b, R \in \mathcal{S}.$$

Thus, the minimizing configuration will be a torus with large radius and small width of its vertical cross-sections.

According to [24] and references therein, a variety of experimental conditions produce DNA toroids of outside diameter 100 nm and hole size of 30 nm in diameter.

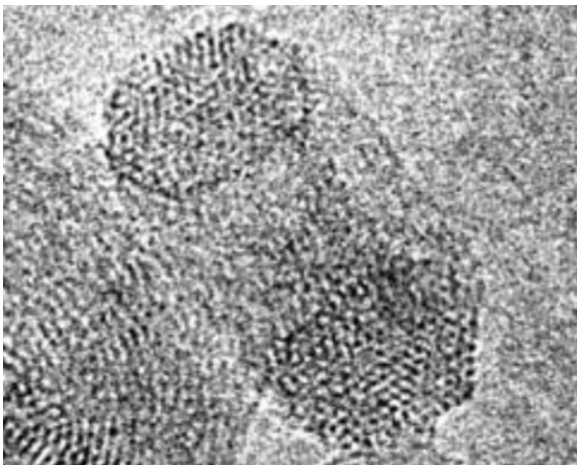

Figure 8: Experimental image of a DNA toroidal condensate from [24]

Using these measurement to determine a value for V_0 and to find initial conditions for b and R, minimizing our energy with $\epsilon_b = 0.05$ gives this configuration with

$$\begin{aligned} a &= 17.55 \text{ nm}, \\ b &= 16.77 \text{ nm}, \\ R &= 33.83 \text{ nm}, \end{aligned}$$

which gives an outside diameter of 101.2 nm and hole size diameter of 34.1 nm.

Minimizing when Surface Forces Dominate

The other case is where the surface interaction energy is far greater than the cost of bending. This case is more akin to LCLC experiments, particularly those where a condensing agent is introduced.

Let $\epsilon_s := K_3/\sigma \ll 1$. The energy is now

$$E_s := E_{chr}/\sigma = \epsilon_s \frac{V_0}{R^2(1+\sqrt{1-b^2/R^2})} + \frac{4V_0}{\pi b} E_e(k). \tag{61}$$

Minimizing (61) as $\epsilon_s \to 0$ amounts to minimizing its second term, so we look at the terms of the gradient with coefficient σ. With the knowledge that $K_e(k) \geq E_e(k)$ for all k, it is clear that

$$\left.\frac{\partial E_s}{\partial R}\right|_{\epsilon_s \to 0} \geq 0, \quad \text{for all } b, R \in \mathcal{S}.$$

To show that $\left.\frac{\partial E_s}{\partial b}\right|_{\epsilon_s \to 0} \leq 0$, we will show

$$\begin{aligned} &\frac{32\pi^3 R^2 b^2}{V_0 k^2}(K_e(k) - E_e(k)) - \frac{4V_0}{\pi b^2} E_e(k) \leq 0 \\ &\implies (1-k^2)\frac{4}{\pi k^2}(K_e(k) - E_e(k)) \leq \frac{2}{\pi} E_e(k). \end{aligned}$$

The following uses [13, Eq. 19.9.4, 19.9.6] which hold for $0 < k < 1$

$$\begin{aligned} (1-k^2)\frac{4}{\pi k^2}(K_e(k) - E_e(k)) &< (1-k^2)^{5/4} \\ &\leq 1 - k^2 \\ &= \left((1-k^2)^{3/2}\right)^{2/3} \\ &\leq \left(\frac{1+(1-k^2)^{3/2}}{2}\right)^{2/3} \\ &< \frac{2}{\pi} E_e. \end{aligned}$$

Therefore, $\left.\frac{\partial E_s}{\partial b}\right|_{\epsilon_s \to 0} \leq 0$ for all $b, R \in \mathcal{S}$. Thus, in this case, the minimum is achieved for R at its smallest value and b at its largest, implying that it occurs on the $R = b$ boundary of $\mathcal{S}$. This is seen experimentally when observing superstructures of a hexagonal columnar phase of chromonic liquid crystal, where bending is mildly resisted but exposure to the solvent is highly unfavorable.

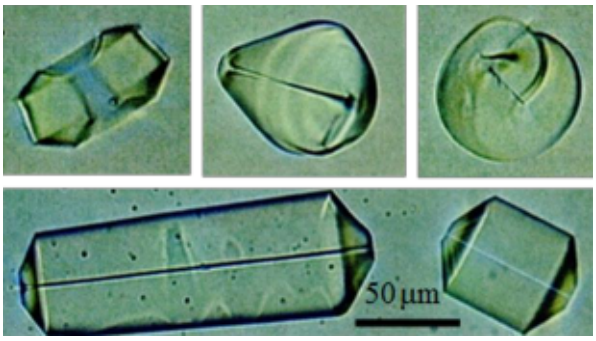

Figure 9: Experimental images of chromonic liquid crystal superstructures

Using the same initial conditions as in the previous case, thinking in μm this time, and setting $\epsilon_s = 0.05$, we find the minimizing configuration is

$$\begin{aligned} a &= 29.22\ \mu\text{m}, \\ b &= 18.45721\ \mu\text{m}, \\ R &= 18.45727\ \mu\text{m}. \end{aligned}$$

Noting that b and R differ by only about 0.00006, this indicates that the center hole will nearly disappear, as is seen in experimental images such as Figure 9.

Here is a table of the intermediate results in either unit.

K_3/σ	a	b	R
$K_3 = 0,\ \sigma = 1$	29.2520	18.4460	18.4460
0.1	28.9096	18.5516	18.5582
1.0	26.6371	19.1047	19.5584
5.0	22.2264	19.0459	23.5120
10.0	19.8736	18.1872	27.5370
$K_3 = 1,\ \sigma = 0$	1.4000	1.4000	5077.7112

Table 4: Dimensions of tori formed for different ratios of K_3/σ.

Note in the last row of the table that we set $d/2 = 1.4$, which we take to be the effective radius of one column and the minimum value for both a and b.

One takeaway from the calculations of this section is that the model is able to aptly predict equilibrium shapes of toroidal aggregates, but another, possibly more important, takeaway is that the constant σ can easily be calibrated in this simpler geometry then be applied in slightly less restrictive scenarios. For example, with a slight adjustment of experimental conditions, scientists could

also appropriately adjust the calibrated value for σ, and predict equilibrium shapes in which the geometry is allowed to deviate from having an elliptic cross-section, possibly attaining another shape.

6.3 Existence of Solutions in a Lipschitz Domain

The aim now is to show existence of minimizers of (12) in a more general domain with a volume constraint. The hope is that this theorem could be used in conjunction with the previous results to relax certain assumptions, like symmetry about a given axis or constraints on shape. We adapt Theorem 9 from [25].

First a definition for a term that appears in Theorem 9:

Definition 4 (From [1])**.** *The perimeter $P_\Omega(A)$ for any Borel set $A \subset \mathbb{R}^n$ is defined by*

$$P_\Omega(A) = \sup\left\{ \int_A \nabla \cdot g \, dx : g \in C_c^1(\Omega; \mathbb{R}^n), |g| \leq 1 \right\}.$$

Theorem 9 (From [25])**.** *Let*

$$I(A, u) = \int_\Omega |\nabla u|^2 dx + P_\Omega(A),$$

where $P_\Omega(A)$ denotes the perimeter of A inside Ω in the sense of de Giorgi. Then, there exists at least one minimizing pair (A, u) such that $u = u_0$ on $\partial\Omega$ for any $u_0 \in H^1(\Omega, \mathbb{R}^n)$, $\mathrm{Vol}(A) = \beta \,\mathrm{Vol}(\Omega)$ for given constant $0 < \beta < 1$, and $u \in \Sigma$ where Σ is a smooth embedded q-dimensional submanifold of $\mathbb{R}^n$ with $0 \leq q < n$.

The proof they give is the following.

Proof from [25]. We use the direct method of the calculus of variations. First let $\tilde{A} \subset\subset \Omega$ be any smooth subset such that $\mathrm{Vol}(\tilde{A}) = \beta \,\mathrm{Vol}(\Omega)$. Let $\tilde{u} \in H^1_{u_0}(\Omega, \mathbb{R}^n)$ be such that $\tilde{u} \equiv P$ in $\tilde{A}$ for some point $P \in \Sigma$ and $\tilde{u}$ is harmonic in $\Omega \setminus \tilde{A}$. Then $(\tilde{A}, \tilde{u})$ is a pair satisfying the constraints and the corresponding energy is finite.

Now let (A_i, u_i) be a minimizing sequence such that $\chi_{A_i} \in BV(\Omega)$ and $u_i \in H^1_{u_0}(\Omega, \mathbb{R}^n)$. Since χ_{A_i} and u_i are uniformly bounded in $BV(\Omega)$ and H^1, respectively, we may assume, by passing to a subsequence if necessary, that $\chi_{A_i} \rightharpoonup \chi_A$ weakly in $BV(\Omega)$ and strongly in $L^1(\Omega)$, and that $u_i \rightharpoonup u$ weakly in $H^1(\Omega, \mathbb{R}^n)$ and strongly in $L^2(\Omega, \mathbb{R}^n)$. Here $A \subset \Omega$ is also a set of finite perimeter.

By lower semicontinuity of the BV norm and Sobolev norm, we have

$$\int_\Omega |\nabla u|^2 + P_\Omega(A) \leq \liminf_{i\to\infty} \int_\Omega |\nabla u_i|^2 + P_\Omega(A_i).$$

Moreover, from the convergence, we have $u \in H^1_{u_0}(\Omega, \mathbb{R}^n)$ and $\mathrm{Vol}(A) = \beta\,\mathrm{Vol}(\Omega)$.

To show that (A, u) is actually a minimizing pair, we only need to check that u maps A into Σ. To see this, by passing to a subsequence again if necessary, we can assume $\chi_{A_i} \to \chi_A$ a.e. and $u_i \to u$ a.e. So for any $x \in A$ such that $\chi_{A_i}(x) \to \chi_A(x)$ and $u_i(x) \to u(x)$, we have $x \in A_i$ for any i sufficiently large, thus $u_i(x) \in \Sigma$. And since Σ is closed, we have $u(x) \in \Sigma$ as we wanted. □

In our case, we consider a system with hexagonal columnar liquid crystal surrounded by isotropic liquid crystal, with tangential surface anchoring at the interface between the two materials.

Let $\mathcal{U} \subset \mathbb{R}^3$ be a bounded Lipschitz domain containing both phases. We aim to find a measurable, Lipschitz subset Ω of $\mathcal{U}$, containing the chromonic phase, with χ_Ω in $BV(\mathcal{U})$ and a function $\mathbf{n}$ in $H^1(\mathcal{U}; \mathbb{R}^3)$ such that the pair $(\mathbf{n}, \Omega)$ minimizes the energy proposed below in (62). This expression accounts for the energy of the isotropic phase in $\mathcal{U} \setminus \Omega$, and both the surface area of and the surface anchoring on $\partial\Omega$:

$$E_{gen}(\mathbf{u}, \widehat{\Omega}) = \int_{\widehat{\Omega}} K_3 |\mathbf{u} \times \nabla \times \mathbf{u}|^2 \, d\mathbf{x} + \nu\,\mathrm{Vol}(\mathcal{U} \setminus \widehat{\Omega}) + \sigma \int_{\partial\widehat{\Omega}} 1 + (\mathbf{u} \cdot \boldsymbol{\nu})^2 \, dS \tag{62}$$

with the constraints

$$\begin{aligned} |\mathbf{u}| &= 1 \text{ in } \widehat{\Omega}, \\ \nabla \cdot \mathbf{u} &= 0 \text{ in } \widehat{\Omega}, \\ \mathbf{u} \cdot \nabla \times \mathbf{u} &= 0 \text{ in } \widehat{\Omega}, \\ \mathrm{trace}(\mathbf{u}) &= \mathbf{n}_0 \text{ on } \partial\widehat{\Omega}, \\ \mathrm{Vol}(\widehat{\Omega}) &= V_0, \quad \text{a constant.} \end{aligned} \tag{63}$$

Let the admissible set be

$$\mathcal{A} = \{(\mathbf{u}, \widehat{\Omega}) \ : \ \mathbf{u} \in H^1(\mathcal{U}; \mathbb{R}^3),\ \chi_{\widehat{\Omega}} \in BV(\mathcal{U}),\ \text{the conditions in (63) are satisfied}\}.$$

Theorem 10. *For any Lipschitz $\mathbf{n}_0$, there exists at least one minimizing pair $(\mathbf{n}, \Omega)$ in $\mathcal{A}$.*

Proof. Let $(\mathbf{n}_k, \Omega_k)$ be a minimizing sequence in $\mathcal{A}$. Since χ_{Ω_k} and $\mathbf{n}_k$ are uniformly bounded in $BV(\mathcal{U})$ and $H^1(\mathcal{U}; \mathbb{R}^3)$, respectively, there exist subsequences (still referred to as χ_{Ω_k} and $\mathbf{n}_k$) that

$\chi_{\Omega_k} \rightharpoonup \chi_\Omega$ weakly in $BV(\mathcal{U})$ and strongly in $L^1(\mathcal{U})$, and $\mathbf{n}_k \rightharpoonup \mathbf{n}$ weakly in $H^1(\mathcal{U};\mathbb{R}^3)$ and strongly in $L^2(\mathcal{U};\mathbb{R}^3)$.

Therefore, trace$(\mathbf{n}) = \mathbf{n}_0$, $|\mathbf{n}| = 1$, Vol$(\Omega) = V_0$ from the convergence in the respective spaces. Also note that, for the sequence of normal vectors $\{\boldsymbol{\nu}_k\}$ to Ω_k, we can pass to (possibly another) subsequence of the same name in which $\boldsymbol{\nu}_k \to \boldsymbol{\nu}$, $\chi_{\Omega_k} \to \chi_\Omega$, and $\mathbf{n}_k \to \mathbf{n}$ pointwise almost everywhere. Then,

$$\lim_{k\to\infty} \int_{\partial\Omega_k} (\mathbf{n}_k \cdot \boldsymbol{\nu}_k)^2 = \int_{\partial\Omega} (\mathbf{n}\cdot\boldsymbol{\nu})^2.$$

By the weak lower semicontinuity of the Oseen-Frank energy, shown in lemma 3, and of the BV norm,

$$E_{gen}(\mathbf{n},\Omega) \le \liminf_{k\to\infty} E_{gen}(\mathbf{n}_k,\Omega_k).$$

By the same arguments as in Theorem 8, the splay and twist constraints are satisfied, and thus the limits $\mathbf{n}$ and Ω are in $\mathcal{A}$ and are a minimizing pair of the energy E_{gen}. □

One way the proof of Theorem 10 differs from that in [25] is that the domain to be minimized must be Lipschitz in order to ensure the normal vector $\boldsymbol{\nu}$ exists almost everywhere.

7 Solutions in a Capsid

This section focuses on using the model from Section 4 to predict the size and shape of the core region of disorder that forms at the center of bacteriophage capsids. Applications involving bacteriophages, including their use in attacking harmful bacteria, require effective ejection properties of the phages, and knowledge of the disordered region becomes useful here; the efficiency of ejection depends on the pressure within the capsid, which in turn, depends on the organization of the DNA.

7.1 Core Radius Size & Capsid Pressure: Free Boundary Model

In order to test the validity of our description in a capsid, we first take a simple geometric setting and use the model E_{cap} and some chosen parameter values to predict the size of the disordered core region and the pressure exerted at the surface of the capsid. The computed values will then be compared to the experimentally measured values for each quantity. We will first retain the parameters K_3, ν, and σ and neglect the elastic energy, by setting $B = 0 = C$. This will lead to good

predictions of the radius but pressures of two orders of magnitude smaller than the experimentally measured ones.

Suppose the capsid is represented as a sphere with radius scaled to be 1, truncated at the poles at a distance $0 < h < 1$, where $h \approx 1$, from the equator. Throughout §7.1, we assume that the core is a truncated prolate spheroid with semiaxes $0 < a < 1$ and 1, with axis aligned with the z-axis. The cross-section of the spheroid in the $xz-$plane is an ellipse given by the equation

$$\frac{x^2}{a^2} + z^2 = 1.$$

Let $\mathcal{B} \subset \mathbb{R}^3$ denote the capsid region and $\Omega_0 \subset \mathcal{B}$ the disordered core. In cylindrical coordinates, they are given by

$$\begin{aligned}
\mathcal{B} &= \{(r, \theta, z) \ : \ 0 \leq r \leq \sqrt{1 - z^2},\ 0 \leq \theta < 2\pi, -h \leq z \leq h\}, \\
\Omega_0 &= \{(r, \theta, z) \ : \ 0 \leq r \leq r_c(z),\ 0 \leq \theta < 2\pi, -h \leq z \leq h\}, \text{ with} \\
r_c &= a\sqrt{1 - z^2}.
\end{aligned}$$

The surface area of the truncated spheroid with semi-axes $\{a, b = 1\}$ is given by

$$\text{Area}\,(\partial\Omega_0) = 2\pi a^2 \left(1 + \frac{1}{a\sqrt{1-a^2}} \arcsin\left(\sqrt{1-a^2}\right)\right) - 2\pi(1-h). \tag{64}$$

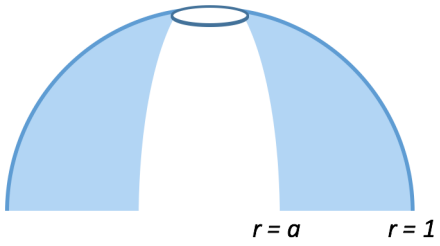

Figure 10: Prescribed capsid geometry

Let $\Omega = \mathcal{B} \setminus \Omega_0$. The DNA configuration is assumed to be a spooling which is concentric in the xy-direction about the z-axis so that $\mathbf{n} = \mathbf{e}_\theta$ almost everywhere, where $\{\mathbf{e}_r, \mathbf{e}_\theta, \mathbf{e}_z\}$ is the standard basis for $\mathbb{R}^3$ in cylindrical coordinates. The remaining quantities, summarized in Tables 1, 2, and 3, include the following: d is the DNA diameter which also plays the role of the interlayer distance in the representation where strands occupy level curve locations (in both the horizontal and vertical directions), L_p is the persistence length of the strand, ν will quantify the energy of the disordered material in the core, and σ will quantify the surface tension between the ordered and disordered

regions. We have discussed their dimensions and typical values in Section 4.

The quantity K_3 in the Oseen-Frank energy is usually a constant determined by the material under consideration. In the setting of the capsid, the DNA behaves like a uniform elastic string, where its total length is two to three orders of magnitude larger than its persistence length, and accordingly, the bend modulus can be written in terms of the persistence length and the linear density m_0 [20]. For K_3, we use the expression given in (34).

Our definition for σ is based on a molecular dynamics expression for the surface tension of rigid rods between nematic and isotropic phases which is

$$\sigma = \beta \frac{K_B T}{L_p d},$$

where d is acting as the diameter of the molecules and the persistence length L_p as the length of a liquid crystal molecule. The particular estimate $\beta = 0.257$ was found from the Onsager theory of rigid rods [15]. In the application of viruses, this factor turns out to be 10 times larger. For the virus T4, we estimate $\beta \approx 2.9$.

For ν, we use

$$\nu = K_B T \nu_0(c)/R_c^3, \quad \nu_0 = \ln\left(\frac{c}{4\pi}\right) - 1 + c \tag{65}$$

where c is the concentration of molecules that has been nondimensionalized by the quantity $4/(\pi d L_p^2)$ [62]. In the molecular theory of Onsager, this expression for ν is the free energy density in the isotropic state.

Therefore, the energy after having imposed the volume constraint (21), and taking into account that the domains Ω, $\mathcal{B}$, and Ω_0 are dimensionless, is

$$\begin{aligned}
\frac{1}{K_B T} E_{cap}(a) &= \int_\Omega \left(\bar{K_3}|\mathbf{n} \times \nabla \times \mathbf{n}|^2 - \bar{\nu}\right) d\mathbf{x} + \bar{\sigma}\,\mathrm{Area}(\partial\Omega_0) + \bar{\nu}\,\mathrm{Vol}(\mathcal{B}) \\
&= \bar{K_3}\left\{ \int_{-h}^{h} \int_{a\sqrt{1-z^2}}^{\sqrt{1-z^2}} \int_0^{2\pi} \left(\frac{1}{2r} - \frac{\bar{\nu}}{\bar{K_3}} r\right) d\theta dr dz + \frac{\bar{\sigma}}{\bar{K_3}}\,\mathrm{Area}(\partial\Omega_0)\right\} + \bar{\nu}\,\mathrm{Vol}(\mathcal{B}) \\
&= \bar{K_3}\pi h\left\{ \ln\left(\frac{1}{a}\right) - \frac{\bar{\nu}}{\bar{K_3}} h_1(a) + \frac{\bar{\sigma}}{\bar{K_3}} h_2(a)\right\} + \bar{\nu}\mathrm{Vol}(\mathcal{B}) + \mathcal{O}(1-h), \qquad (66) \\
h_1(a) &= \left(1 - \frac{1}{12}h^2\right)(1-a^2), \qquad (67) \\
h_2(a) &= \frac{2a}{h}\left(a + \frac{1}{\sqrt{1-a^2}} \arcsin\left(\sqrt{1-a^2}\right)\right). \qquad (68)
\end{aligned}$$

A simple modification of the previous expression, that replaces $\bar{K_3}$ with $(1+\delta)\bar{K_3}$ and includes the terms multiplying $\bar{K}$ in (29), yields the energy expression in the case that the cross-sectional

elastic contribution is included. If we consider the DNA as a stiff filament but neglect transverse interactions, then the bending constant is K_3. However, when the transverse energy is accounted for, it effectively results in a larger bending modulus $A = K_3(1+\delta)$. In the same vein, we assume that the effective values of the other parameters carry this factor of $1+\delta$. These look like

$$\tilde{\nu} = \bar{\nu}(1+\delta), \quad \tilde{\sigma} = \bar{\sigma}(1+\delta)$$

Including this elastic energy also accounts for the electrostatic forces between adjacent segments, which contribute in both the ordered and disordered phases. We further suppress the last two constant terms in the previous expression of the energy, and denote the dimensionless energy as follows:

$$\begin{aligned}\mathcal{E}(a) &= (1+\delta)\bar{K}_3\pi h\left\{\left(1+\frac{2\delta}{1+\delta}\right)\ln\left(\frac{1}{a}\right) - \frac{\tilde{\nu}}{(1+\delta)\bar{K}_3}h_1(a) + \frac{\tilde{\sigma}}{(1+\delta)\bar{K}_3}h_2(a)\right\} \\ &= (1+\delta)\bar{K}_3\pi h\left\{\left(1+\frac{2\delta}{1+\delta}\right)\ln\left(\frac{1}{a}\right) - \frac{\bar{\nu}}{\bar{K}_3}h_1(a) + \frac{\bar{\sigma}}{\bar{K}_3}h_2(a)\right\}. \end{aligned} \tag{69}$$

Before proceeding to minimizing the energy, let us revise the form of the nondimensional groups $\tilde{\nu}/\bar{K}_3$ and the analogous one for σ. For this, we write down the dimensionless versions of the parameters in the energy equation:

$$\frac{\bar{\nu}}{\bar{K}_3} = \dim\left(\frac{\nu}{K_3}\right) = \frac{\pi\nu_0(c)}{L_pL}L_0^2, \quad \frac{\bar{\sigma}}{\bar{K}_3} = \dim\left(\frac{\sigma}{K_3}\right) = \beta\pi\frac{R_c^3}{L_p^2Ld}L_0, \tag{70}$$

where L_0 is a typical length scale that we choose so that

$$\dim\left(\frac{\nu}{K_3}\right) = \dim\left(\frac{\sigma}{K_3}\right) = 1.$$

In particular, we take

$$L_0^2 = \frac{LpL}{\pi\nu_0(c)}.$$

The previous energy reduces then to

$$(1+\delta)\bar{K}_3\pi h\left\{\left(1+\frac{2\delta}{1+\delta}\right)\ln\left(\frac{1}{a}\right) - h_1(a) + \beta\sigma_0 h_2(a)\right\}, \tag{71}$$

where

$$\sigma_0 = \frac{R_c^3}{L_p^{3/2}L^{1/2}d\nu_0(c)^{1/2}}, \quad \alpha = \left(1+\frac{2\delta}{1+\delta}\right).$$

Let us use the virus $\epsilon 15$ as benchmark, and take a typical pressure of 35 atm, gives $\delta = 70$.

Then

$$\alpha = \left(1 + \frac{2\delta}{1+\delta}\right) = \left(1 + \frac{140}{71}\right) = 2.9718.$$

Virus	$\nu_0(c)$	σ_0	$p_B(atm)$	β	r_c exp (nm)	r_c model (nm)	error (%)
T4	23.19	0.057	0.388	3.1	22.00	22.80	3.5
T5	19.04	0.065	0.228	3.1	17.64	21.48	17
T7	19.82	0.034	0.592	3.1	15.34	16.15	5.0
ϵ15	15.37	0.052	0.499	3.1	16.25	16.17	0.5

Table 5: The dimensionless quantities $\nu_0(c)$ and σ_0 represent the expressions in the corresponding moduli that depend on the geometry of the system. β is a parameter, that, in the case of systems of rigid rods is calculated using Onsager's theory. The lack of a theory of this type for DNA prompted us to search for appropriate fitting values. For the T5 virus, with the largest capsid in the group, a good parameter fit is $\beta = 5.5$ that gives $r_c = 17.22$.

Here, we present the plots of the energy functions (71), precisely, the expression between braces.

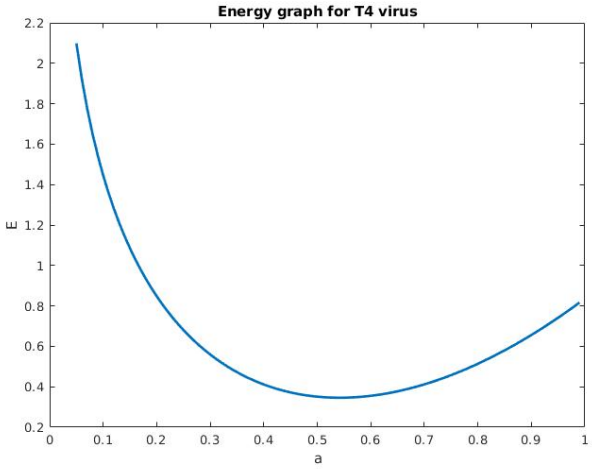

Figure 11: Energy graph for T4-virus. In this plot, we take $\beta = 3.0$ with the minimum corresponding to $r_c = 21.7$ nm.

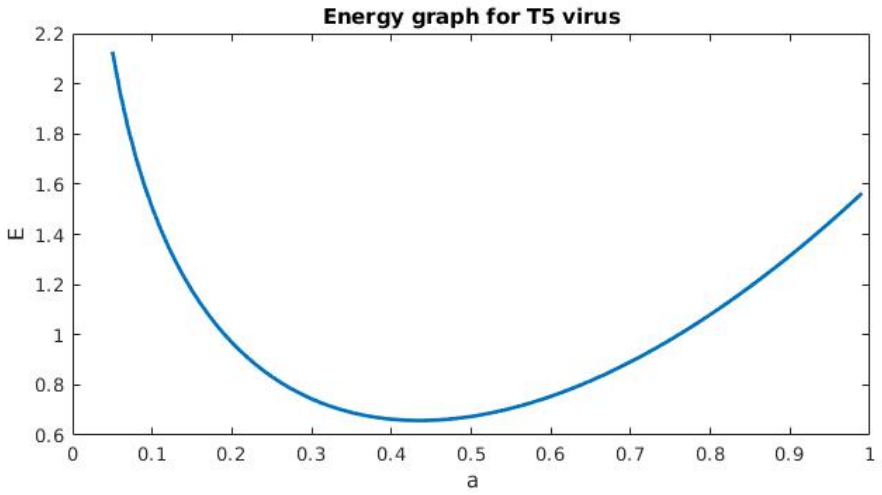

Figure 12: Energy graph for T5-virus. In this plot, we take $\beta = 5.5$ with the minimum corresponding to $r_c = 17.22$ nm.

Note that the original capsid energy results from setting $\delta = 0$ in the previous one, in which case only the penalty to bending is included in the ordered region of the capsid. Even with the scaling of ν and σ, we still see the contribution of the elastic moduli in the factor in front of the bending energy. For parameters values from the tables in §4.4, and taking $\delta = 400$, the graphs for the different viruses show an absolute minimum in the range of a between 0.3 and 0.6.

Pressure Estimates. Another test of the capsid model is its ability to predict the forces within a bacteriophage capsid. To do so, we begin with a calculation of the Cauchy stress tensor associated with the total energy (20) using a standard variational argument. Quantities obtained from the stress tensor will give the pressure at a point in Ω, the force tangent to the DNA filament, and the force that is responsible for its ejection.

The Cauchy stress tensor T results from the first variation of the free energy of a system with respect to the deformation of the material, keeping the layer positions and director orientation fixed [64]. Let Ω_r be the reference domain and Ω be the present liquid crystal configuration.

Let us calculate the tensor associated to the Oseen-Frank energy (4). Suppose $\mathbf{X}$ denotes a point in Ω_r and $\mathbf{x}$ denotes a point in Ω. The deformation will be represented by sending $\mathbf{x} \mapsto \mathbf{x} + \delta\mathbf{x}$. Let $F = \nabla_{\mathbf{X}}\mathbf{x}$ and $J = \det(F)$. The symbol δ_x will signify the difference between the deformed and undeformed states.

Therefore the change in the Oseen-Frank energy due to deformation is the following:

$$\begin{aligned}
\delta_x E_{OF} &= \delta_x \int_\Omega W_{OF}\, d\mathbf{x} \\
&= \delta_x \int_{\Omega_r} W_{OF}\, J\, d\mathbf{X} \\
&= \int_{\Omega_r} \delta_x(W_{OF}J)\, d\mathbf{X} \\
&= \int_\Omega \delta_x(W_{OF}J)\, J^{-1} d\mathbf{x} \\
&= \int_\Omega \left[\frac{\partial W_{OF}}{\partial \mathbf{n}} \delta_x \mathbf{n} + \frac{\partial W_{OF}}{\partial \nabla \mathbf{n}} \delta_x(\nabla \mathbf{n}) + W_{OF} \delta_x J\, J^{-1} \right] d\mathbf{x}.
\end{aligned}$$

The following calculations will help us to simplify:

$$\begin{aligned}
\delta_x \mathbf{n} &= 0, \\
\delta_x(\nabla \mathbf{n}) &= \nabla_{\mathbf{X}} \mathbf{n} \delta_x(F^{-1}) = -\nabla_{\mathbf{X}} \mathbf{n} F^{-1} \nabla \delta \mathbf{x} = -\nabla \mathbf{n} \nabla \delta \mathbf{x}, \\
\delta_x J &= \det(F + \nabla_{\mathbf{X}} \delta \mathbf{x}) - \det(F) \\
&= \det(F) \left(\det(I + \nabla_{\mathbf{X}} \delta \mathbf{x} F^{-1}) - 1 \right) \\
&= \det(F) \left(\det(I + \nabla \delta \mathbf{x}) - 1 \right) \\
&= \det(F) \left(1 + \operatorname{tr}(\nabla \delta \mathbf{x}) + \mathcal{O}(|\delta \mathbf{x}|^2) - 1 \right) \\
&= J(\nabla \cdot \delta \mathbf{x}) + \mathcal{O}(|\delta \mathbf{x}|^2).
\end{aligned}$$

Considering the above and neglecting higher order terms in $|\delta \mathbf{x}|$, the change is

$$\begin{aligned}
\delta_x E_{OF} &= \int_\Omega \left[-\frac{\partial W_{OF}}{\partial \nabla \mathbf{n}} \, : \, \nabla \mathbf{n} \nabla \delta \mathbf{x} + W_{OF}(\nabla \cdot \delta \mathbf{x}) \right] d\mathbf{x} \\
&= \int_\Omega \left[-(\nabla \mathbf{n})^T \frac{\partial W_{OF}}{\partial \nabla \mathbf{n}} + W_{OF}(\mathbf{n}, \nabla \mathbf{n}) I \right] : \nabla \delta \mathbf{x}\, d\mathbf{x} \\
&:= \int_\Omega T_{OF} : \nabla \delta \mathbf{x}.
\end{aligned}$$

where I is the identity tensor.

Returning to the test case outlined above, where $\mathbf{n} = \mathbf{e}_\theta$, we first calculate the Cauchy stress tensor for the energy (20) without the elastic energy terms of the cross-sections.

In this case, the stress is

$$\begin{aligned} T_{OF} &= -(\nabla \mathbf{n})^T \frac{\partial W_{OF}}{\partial \nabla \mathbf{n}} + W_{OF}(\mathbf{n}, \nabla \mathbf{n}) I \\ &= -(\nabla \mathbf{n})^T \left[8K_3 \left(\frac{1}{2}(\nabla \mathbf{n} - (\nabla \mathbf{n})^T) \right) \mathbf{n} \otimes \mathbf{n} \right]_{skew} \\ &\quad + K_3 |\mathbf{n} \times (\nabla \times \mathbf{n})|^2 I. \end{aligned} \tag{72}$$

Substituting $\mathbf{e}_\theta$ for $\mathbf{n}$, the above simplifies to

$$-(\nabla \mathbf{n})^T \left[8K_3 \left(\frac{1}{2}(\nabla \mathbf{n} - (\nabla \mathbf{n})^T) \right) \mathbf{n} \otimes \mathbf{n} \right]_{skew} = \begin{pmatrix} 0 & 0 & 0 \\ 0 & -\frac{2K_3}{r^2} & 0 \\ 0 & 0 & 0 \end{pmatrix}.$$

Therefore,

$$T_{OF} = \begin{pmatrix} 0 & 0 & 0 \\ 0 & -\frac{2K_3}{r^2} & 0 \\ 0 & 0 & 0 \end{pmatrix} + \begin{pmatrix} \frac{K_3}{r^2} & 0 & 0 \\ 0 & \frac{K_3}{r^2} & 0 \\ 0 & 0 & \frac{K_3}{r^2} \end{pmatrix} = \begin{pmatrix} \frac{K_3}{r^2} & 0 & 0 \\ 0 & -\frac{K_3}{r^2} & 0 \\ 0 & 0 & \frac{K_3}{r^2} \end{pmatrix} \tag{73}$$

In this test case, there are no shear forces; the stress is purely in the form of a pressure, as is shown below.

Using this expression for the Cauchy stress tensor T_{OF}, we can derive expressions for the forces within the capsid. Let

$$\boldsymbol{\nu} = r\mathbf{e}_r + z\mathbf{e}_z = r\mathbf{e}_r + \sqrt{1 - r^2}\mathbf{e}_z$$

be a unit outward normal on the surface of Ω, recalling that the sphere is scaled to have radius 1. The pressure is then defined as

$$T_{OF}\boldsymbol{\nu} \cdot \boldsymbol{\nu} = K_3 \begin{pmatrix} \frac{1}{r^2} & 0 & 0 \\ 0 & -\frac{1}{r^2} & 0 \\ 0 & 0 & \frac{1}{r^2} \end{pmatrix} \begin{pmatrix} r \\ 0 \\ \sqrt{1 - r^2} \end{pmatrix} \cdot \begin{pmatrix} r \\ 0 \\ \sqrt{1 - r^2} \end{pmatrix} = \frac{K_3}{r^2}. \tag{74}$$

Therefore, the pressure at any (cylindrical) radius $r_c \leq r \leq 1$ within Ω is given by $p(r) = K_3/r^2$. The force tangent to the DNA strand is given by

$$T_{OF}\boldsymbol{\nu} \cdot \mathbf{n} = K_3 \begin{pmatrix} \frac{1}{r^2} & 0 & 0 \\ 0 & -\frac{1}{r^2} & 0 \\ 0 & 0 & \frac{1}{r^2} \end{pmatrix} \begin{pmatrix} r \\ 0 \\ \sqrt{1 - r^2} \end{pmatrix} \cdot \begin{pmatrix} 0 \\ 1 \\ 0 \end{pmatrix} = 0, \tag{75}$$

which is expected when there are no shear forces.

Last, we calculate the force along the director to find the force of ejection. This force is

$$T_{OF}\mathbf{n}\cdot\mathbf{n} = K_3 \begin{pmatrix} \frac{1}{r^2} & 0 & 0 \\ 0 & -\frac{1}{r^2} & 0 \\ 0 & 0 & \frac{1}{r^2} \end{pmatrix} \begin{pmatrix} 0 \\ 1 \\ 0 \end{pmatrix} \cdot \begin{pmatrix} 0 \\ 1 \\ 0 \end{pmatrix} = -\frac{K_3}{r^2}. \tag{76}$$

Measurements of the pressure and force of ejection of a virus are gathered by placing viruses in a solution of PEG (polyethylene glycol) along with proteins that trigger ejection. The concentration of the PEG can be used to estimate the force of ejection and pressure within a viral capsid. Graphs such as those in Figure 13, found in [22], show the relationship between external osmotic pressure, PEG concentration, and percentage of genome length ejected. It should be noted here that the pressures measured in experiments depends on PEG concentration, which our models do not currently account for. This feature is discussed in §8.1.

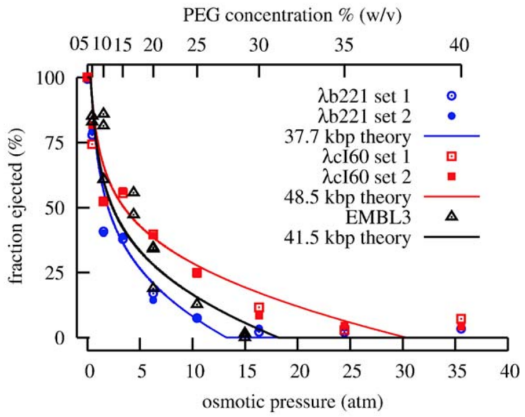

Figure 13: DNA ejection as a function of osmotic pressure for two strains of λ phages

Let us estimate the pressure on the capsid surface, in Pascal units,

$$p_B := K_B T m_0 \frac{L_p}{R_c^2}.$$

This pressure deficiency is due to having neglected the cross-sectional elasticity from our calculation. To include the cross-sectional energy, we can proceed exactly as above but with the density from (29), which is

$$\mathcal{W}(\mathbf{n}, \nabla\mathbf{n}) := A\left(|\mathbf{n}\times\nabla\times\mathbf{n}|^2 + K\left(\mathrm{tr}(\nabla\mathbf{n})^2 + (\mathbf{n}\cdot\nabla\times\mathbf{n})^2\right) - \frac{\nu}{A}\right). \tag{77}$$

h

Virus	Pressure (atm)
T4	0.388
T5	0.228
T7	0.592
ϵ15	0.499

Table 6: Pressure is underpredicted in the absence of the elastic energy

Then the stress tensor is

$$\begin{aligned} T &= -(\nabla \mathbf{n})^T \frac{\partial \mathcal{W}}{\partial \nabla \mathbf{n}} + \mathcal{W}(\mathbf{n}, \nabla \mathbf{n}) I \\ &= A\Big\{ -(\nabla \mathbf{n})^T \left[8 \left(\frac{1}{2}(\nabla \mathbf{n} - (\nabla \mathbf{n})^T) \right) \mathbf{n} \otimes \mathbf{n} \right]_{skew} \\ &\quad - 2K(\nabla \mathbf{n})^T \left[(\nabla \mathbf{n})^T + (\mathbf{n} \cdot \nabla \times \mathbf{n}) \operatorname{rot}(\mathbf{n}) \right] \\ &\quad + \left(|\mathbf{n} \times \nabla \times \mathbf{n}|^2 + K \left(\operatorname{tr}(\nabla \mathbf{n})^2 + (\mathbf{n} \cdot \nabla \times \mathbf{n})^2 \right) - \frac{\nu}{A} \right) I \Big\}, \end{aligned} \tag{78}$$

where $\operatorname{rot}(\mathbf{n})\mathbf{u} := \mathbf{n} \times \mathbf{u}$ for any vector $\mathbf{u} \in \mathbb{R}^3$.

Now, in the test case $\mathbf{n} = \mathbf{e}_\theta$,

$$-(\nabla \mathbf{n})^T \left[8 \left(\frac{1}{2}(\nabla \mathbf{n} - (\nabla \mathbf{n})^T) \right) \mathbf{n} \otimes \mathbf{n} \right]_{skew} = \begin{pmatrix} 0 & 0 & 0 \\ 0 & -\frac{2}{r^2} & 0 \\ 0 & 0 & 0 \end{pmatrix}$$

$$-2K(\nabla \mathbf{n})^T \left[(\nabla \mathbf{n})^T + (\mathbf{n} \cdot \nabla \times \mathbf{n}) \operatorname{rot}(\mathbf{n}) \right] = \begin{pmatrix} 0 & 0 & 0 \\ 0 & 0 & 0 \\ 0 & 0 & 0 \end{pmatrix}$$

$$\left(|\mathbf{n} \times \nabla \times \mathbf{n}|^2 + K \left(\operatorname{tr}(\nabla \mathbf{n})^2 + (\mathbf{n} \cdot \nabla \times \mathbf{n})^2 \right) - \frac{\nu}{A} \right) I = \begin{pmatrix} \frac{1}{r^2} - \frac{\nu}{A} & 0 & 0 \\ 0 & \frac{1}{r^2} - \frac{\nu}{A} & 0 \\ 0 & 0 & \frac{1}{r^2} - \frac{\nu}{A} \end{pmatrix}.$$

Thus, summing the above terms,

$$T = A \begin{pmatrix} \frac{1}{r^2} - \frac{\nu}{A} & 0 & 0 \\ 0 & -\frac{1}{r^2} - \frac{\nu}{A} & 0 \\ 0 & 0 & \frac{1}{r^2} - \frac{\nu}{A} \end{pmatrix}, \tag{79}$$

and the pressure is

$$T\boldsymbol{\nu}\cdot\boldsymbol{\nu} = A\begin{pmatrix} \frac{1}{r^2}-\frac{\nu}{A} & 0 & 0 \\ 0 & -\frac{1}{r^2}-\frac{\nu}{A} & 0 \\ 0 & 0 & \frac{1}{r^2}-\frac{\nu}{A} \end{pmatrix}\begin{pmatrix} r \\ 0 \\ \sqrt{1-r^2} \end{pmatrix}\cdot\begin{pmatrix} r \\ 0 \\ \sqrt{1-r^2} \end{pmatrix} = A\left(\frac{1}{r^2}-\frac{\nu}{A}\right). \tag{80}$$

We saw in Table 6 that when the cross-sectional elasticity is omitted, and the pressure is controlled primarily by the constant K_3, that the pressures were under predicted. Now, as is evident in (80), the pressure with the presence of those elastic terms is controlled by A, which had the form

$$A = K_3 + B + C,$$

with B and C being the bulk and shear moduli, respectively.

Appealing to relations (29) and (31) and assuming ν/A is small, the resulting pressure is approximately

$$p = (1+\delta)p_B. \tag{81}$$

In particular, for the T4 virus, and taking $\alpha = 10$ as shown in (28), we get

$$p = 41.44 \text{ atm}, \tag{82}$$

which is exactly in the proper range.

7.2 Free Inner Boundary

In images of bacteriophages, like that in Figure 14, it appears that the disordered core region is a spheroidal region surrounded by ordered material. Therefore, we now aim to use the energy E_{cap} in the case where the inner boundary separating the disordered region of DNA from the well-organized region is unknown and the outer boundary of the capsid is fixed.

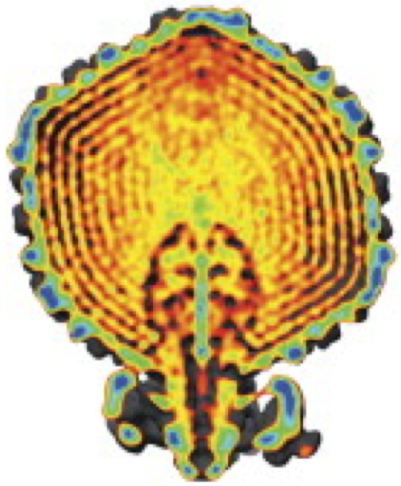

Figure 14: Cryoelectron microscopy image of the bacteriophage $\epsilon 15$, [27]

To set up the problem, we consider a semicircular region with center at the origin. The spherical coordinates (r, ϕ) are used to describe this two-dimensional cross-section, and this cross-section will be revolved in the direction of the coordinate θ to form a three-dimensional hemisphere. An axisymmetric region is removed, whose boundary is given by a function $p(\phi)$ satisfying $p(\pi/2) = r_0$ (see Figure 15). In this case, the function p defines the free boundary.

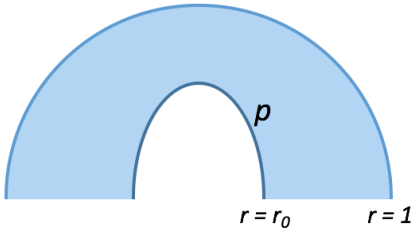

Figure 15: Visualization of free boundary

The energy E_{cap} from (20) in the three-dimensional hemisphere Ω, formed by revolving the two-dimensional cross-section about the z-axis, would be of the following form

$$E_{cap} = \int_0^{2\pi} \int_{\phi^*}^{\pi/2} \int_{p(\phi)}^{1} W_{OF}(\mathbf{n}, \nabla \mathbf{n})\, r^2 \sin\phi \; dr d\phi d\theta + \nu \,\mathrm{Vol}(\Omega_0) + \sigma \,\mathrm{Area}(\partial\Omega_0), \qquad (83)$$

where Ω_0 is the region formed by revolving the area under p about the z-axis. The lower bound ϕ^* comes from the results of [61] which states there is a small cylinder of empty space above the disordered core region where the pressure goes to zero. The value $\phi^* = 0.05$ corresponds to the ratio of DNA length L to persistence length L_p of $L/L_p = 290$. This ratio for viruses T4 and T5 is

much larger and thus corresponds to a lower value for ϕ^*.

It should be noted that in choosing to include the whole of W_{OF}, which includes K_1, K_2, and K_3 terms, we make the assumption that $K_1, K_2 \gg K_3$ to relax the splay and twist constraints. In other words, for example, saying that K_1 is large in the term

$$\int_\Omega K_1(\nabla \cdot \mathbf{n})^2 \, d\mathbf{x}$$

is a relaxation of the pointwise constraint $\nabla \cdot \mathbf{n} = 0$ in Ω from (14).

Suppose, as before, we let $\mathcal{B}$ be the capsid domain and let $\Omega := \mathcal{B} \setminus \Omega_0$. Then the volume constraint from (21) can be rearranged as

$$\mathrm{Vol}(\Omega_0) = \mathrm{Vol}(\mathcal{B}) - \mathrm{Vol}(\Omega).$$

Therefore, we can rewrite (83), after substituting the volume constraint, as

$$E_{cap} = \int_0^{2\pi} \int_{\phi^*}^{\pi/2} \int_{p(\phi)}^1 (W_{OF}(\mathbf{n}, \nabla\mathbf{n}) - \nu) \; r^2 \sin\phi \, dr d\phi d\theta + \sigma \, \mathrm{Area}(\partial\Omega_0) + \nu \, \mathrm{Vol}(\mathcal{B}) \quad (84)$$

to impose the constraint directly. Notice that $\mathrm{Vol}(\mathcal{B})$ is a constant since the outer boundary of the capsid is taken to be of a fixed size. Therefore, in what follows, we analyze a modified energy where this constant is removed, which is

$$\tilde{E}_{cap} = \int_0^{2\pi} \int_{\phi^*}^{\pi/2} \int_{p(\phi)}^1 (W_{OF}(\mathbf{n}, \nabla\mathbf{n}) - \nu) \; r^2 \sin\phi \, dr d\phi d\theta + \sigma \, \mathrm{Area}(\partial\Omega_0). \quad (85)$$

We consider liquid crystal configurations of the form $\mathbf{n} = \sin\varphi \mathbf{e}_\phi + \cos\varphi \mathbf{e}_\theta$, where $\varphi = \varphi(r, \phi)$ is the angle of the molecules at (r, ϕ, θ) from horizontal. The energy in terms of φ is the following

$$\begin{aligned}\tilde{E}_{cap} = \int_\Omega \Bigg\{ &\frac{K_1}{r^2} \left(\cos\varphi\varphi_\phi + \sin\varphi \frac{\cos\phi}{\sin\phi} \right)^2 + K_2 \varphi_r^2 \\ &+ \frac{K_3}{r^2} + \frac{K_3}{r^2} \left(\sin\varphi\varphi_\phi - \cos\varphi \frac{\cos\phi}{\sin\phi} \right)^2 - \nu \Bigg\} \, r^2 \sin\phi dr d\phi d\theta \\ &+ 2\pi\sigma \int_{\phi^*}^{\pi/2} p\sqrt{p^2(\phi) + (p'(\phi))^2} \sin\phi \, d\phi.\end{aligned}$$

In order to minimize the energy $\tilde{E}_{cap}$ and to determine p, we define a coordinate transformation for r that removes p from the integral bounds, assuming that p is sufficiently smooth. This transformed coordinate s is defined so that the outer radius $r = 1$ is fixed and so that the free boundary p is

mapped to a constant radius r_0, as in Figure 16. Thus,

$$\frac{\partial s}{\partial r} = c(1-r) \implies s(r) = -c_1(1-r)^2 + c_2$$

and

$$s(p) = r_0 \quad \& \quad s(1) = 1 \implies c_1 = \frac{1-r_0}{(1-p)^2},\ c_2 = 1.$$

Therefore, $s = 1 - (1-r_0)(1-r)^2/(1-p)^2$ and the new coordinates (s, ϕ, θ) are related to the previous coordinates (r, ϕ, θ) by

$$\begin{aligned} r &= 1 - \sqrt{(1-s)(1-p)^2/(1-r_0)}, \\ \phi &= \phi, \\ \theta &= \theta. \end{aligned}$$

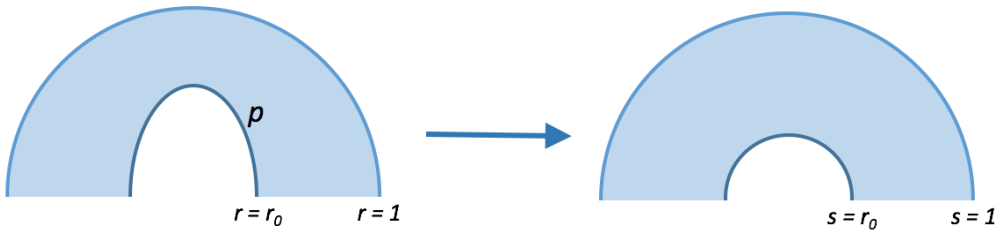

Figure 16: Visualization of coordinate change

In these coordinates,

$$\tilde{E}_{cap} = \int_0^{2\pi} \int_{\phi^*}^{\pi/2} \int_{r_0}^{1} (W_{OF}(\mathbf{n}, \nabla \mathbf{n}) - \nu)\ r^2(s) \frac{\partial r}{\partial s} \sin\phi\, ds d\phi d\theta + \sigma\, \text{Area}(\partial\Omega_0). \tag{86}$$

With the coordinate transformation defined above and $\varphi(r, \phi) \mapsto \hat{\varphi}(s(r, \phi), \phi)$, then

$$\varphi_r = \hat{\varphi}_s \frac{\partial s}{\partial r}, \qquad \varphi_\phi = \hat{\varphi}_s \frac{\partial s}{\partial \phi} + \hat{\varphi}_\phi = \frac{2(1-s)p'}{(1-p)} \hat{\varphi}_s + \hat{\varphi}_\phi.$$

So the Oseen-Frank energy terms become

$$\tilde{E}_{cap} = \int_\Omega \Bigg\{ K_1 \left[\cos\hat{\varphi} \left(\hat{\varphi}_s \frac{\partial s}{\partial \phi} + \hat{\varphi}_\phi \right) + \sin\hat{\varphi}\cot\phi \right]^2 + K_2 r^2(s) \left(\hat{\varphi}_s \frac{\partial s}{\partial r} \right)^2$$
$$+ K_3 + K_3 \left[\sin\hat{\varphi} \left(\hat{\varphi}_s \frac{\partial s}{\partial \phi} + \hat{\varphi}_\phi \right) - \cos\hat{\varphi}\cot\phi \right]^2 - \nu r^2(s) \Bigg\} \frac{\partial r}{\partial s} \sin\phi \, ds d\phi d\theta$$
$$+ 2\pi\sigma \int_{\phi^*}^{\pi/2} p\sqrt{p^2(\phi) + (p'(\phi))^2} \, \sin\phi d\phi$$

$$= \int_\Omega \Bigg\{ K_1 \left[\cos\hat{\varphi} \left(\frac{-2(1-s)}{1-p}(-p'\hat{\varphi}_s) + \hat{\varphi}_\phi \right) + \sin\hat{\varphi}\cot\phi \right]^2 +$$
$$+ K_2 \left(\frac{2\sqrt{(1-r_0)(1-s)}}{1-p} - 2(1-s) \right)^2 \hat{\varphi}_s^2 + K_3 +$$
$$+ K_3 \left[\sin\hat{\varphi} \left(\frac{-2(1-s)}{1-p}(-p'\hat{\varphi}_s) + \hat{\varphi}_\phi \right) - \cos\hat{\varphi}\cot\phi \right]^2$$
$$- \nu \left(1 - \sqrt{\frac{1-s}{1-r_0}}(1-p) \right)^2 \Bigg\} \frac{\sin\phi(1-p)}{2\sqrt{(1-r_0)(1-s)}} ds d\phi d\theta$$
$$+ \int_\Omega \frac{\sigma}{1-r_0} p\sqrt{p^2(\phi) + (p'(\phi))^2} \, \sin\phi ds d\phi d\theta \tag{87}$$
$$:= \int_\Omega \tilde{W}_{cap} \, ds d\phi d\theta. \tag{88}$$

In order to verify the existence of minimizing pairs $(p, \hat{\varphi})$, we will use a result like Theorem 4 stating that coercivity and polyconvexity of a functional imply the existence of minimizers. Recall the definition for polyconvexity from Definition 3 in §2.1:

Definition 3 (Restated)**.** *A Lagrangian L is called polyconvex if L has the form*

$$L(P, \mathbf{z}, \mathbf{x}) = F(P, \det P, \mathbf{z}, \mathbf{x}), \quad P \in M^{n\times n}, \quad \mathbf{z} \in \mathbb{R}^n, \quad \mathbf{x} \in \Omega$$

and for each fixed $\mathbf{z}$, $\mathbf{x}$, the joint mapping $(P, r) \mapsto F(P, r, \mathbf{z}, \mathbf{x})$ is convex.

Then, to match our setup with the definition above,

$$L = \tilde{W}_{cap}, \quad \mathbf{z} = (p, \hat{\varphi}), \quad \mathbf{x} = (s, \phi), \quad P = \begin{pmatrix} 0 & p'(\phi) \\ \hat{\varphi}_s & \hat{\varphi}_\phi \end{pmatrix}, \quad \det P = -p'\hat{\varphi}_s. \tag{89}$$

The following lemma provides a way to verify if the Lagrangian $\tilde{W}_{cap}$ is polyconvex.

Lemma 8. *Let f be a twice-differentiable function on an open convex set $U \subset \mathbb{R}^n$. Then $f(\mathbf{u}, \mathbf{x})$ is convex with respect to $\mathbf{u}$ on U if and only if its Hessian matrix is positive semidefinite for every $\mathbf{x} \in U$.*

We are now set up to show the Lagrangian is polyconvex with respect to P. One thing that may stand out in (89) is that in the definition of P, one entry of the matrix is zero. If we were to show polyconvexity with an arbitrary entry, say p_s, it would result in a row and column of all zeros in the Hessian since no such terms appear in $\tilde{W}_{cap}$ and not provide any insights. Therefore, that entry remains set to zero. We can use the above lemma and (89) to show the following:

Lemma 9. *The Lagrangian $\tilde{W}_{cap}$ of $\tilde{E}_{cap}$ is polyconvex with respect to the gradient of (p, φ).*

Proof. To show polyconvexity, we find the Hessian of $\tilde{W}_{cap}$ with respect to the variables $(p', \hat{\varphi}_s, \hat{\varphi}_\phi, -p'\hat{\varphi}_s)$, and show that the eigenvalues are nonnegative. Let

$$\ell := \frac{\sin\phi}{2\sqrt{(1-r_0)(1-s)(1-p)^2}}$$

Then, the nonzero terms of the Hessian are

$$\begin{aligned}
\frac{\partial^2 \tilde{W}_{cap}}{\partial p'^2} &= \frac{\sigma}{1-r_0}\frac{p^3}{(p^2+(p')^2)^{3/2}}\sin\phi, \\
\frac{\partial^2 \tilde{W}_{cap}}{\partial \hat{\varphi}_s^2} &= 8K_2\left(\sqrt{(1-r_0)(1-s)} - (1-s)(1-p)\right)^2 \ell, \\
\frac{\partial^2 \tilde{W}_{cap}}{\partial \hat{\varphi}_\phi^2} &= 2(1-p)^2(K_1\cos^2\hat{\varphi} + K_3\sin^2\hat{\varphi})\ell, \\
\frac{\partial^2 \tilde{W}_{cap}}{\partial \hat{\varphi}_\phi \partial(-p'\hat{\varphi}_s)} = \frac{\partial^2 \tilde{W}_{cap}}{\partial(-p'\hat{\varphi}_s)\partial\hat{\varphi}_\phi} &= -4(1-s)(1-p)(K_1\cos^2\hat{\varphi} + K_3\sin^2\hat{\varphi})\ell, \\
\frac{\partial^2 \tilde{W}_{cap}}{\partial(-p'\hat{\varphi}_s)^2} &= 8(1-s)^2(K_1\cos^2\hat{\varphi} + K_3\sin^2\hat{\varphi})\ell.
\end{aligned}$$

Therefore, replacing ℓ with its full expression, the matrix has eigenvalues

$$\begin{aligned}
\lambda_1 &= 0,\\
\lambda_2 &= \frac{\sigma}{1-r_0}\frac{p^3}{(p^2+(p')^2)^{3/2}}\sin\phi,\\
\lambda_3 &= \frac{\sin\phi}{2\sqrt{(1-r_0)(1-s)(1-p)^2}}\cdot\left(8(1-s)^2+2(1-p)^2\right)\left(K_1\cos^2\hat{\varphi}+K_3\sin^2\hat{\varphi}\right),\\
\lambda_4 &= \frac{\sin\phi}{2\sqrt{(1-r_0)(1-s)(1-p)^2}}\cdot 8K_2\left(\sqrt{(1-r_0)(1-s)}-(1-s)(1-p)\right)^2,
\end{aligned}$$

and the $\sin\phi$ factor is nonnegative since $0<\phi\leq\pi/2$.

Being that all of the eigenvalues are nonnegative, we can conclude that the Hessian is positive semidefinite and that the Lagrangian is polyconvex with respect to the noted variables. □

With this result in place, the next steps are to determine appropriate boundary conditions for p and φ and to show that there exist minimizers satisfying those and the constraints of the model. The boundary conditions for the DNA are naturally enforced on the outer boundary by the proteins of the capsid wall, so we use images as a guide when choosing the conditions for φ. The condition for p' below ensures that upon reflection across the $z=0$ axis, there will be no cusps on the boundary of Ω_0. We impose the following boundary conditions:

$$\begin{aligned}
p(\pi/2)=r_0, \quad & p'(\pi/2)=0,\\
\varphi(r,\phi^*)=0, \quad & \varphi(r,\pi/2)=0,\\
\varphi(1,\phi)=0, \quad & \frac{\partial\varphi}{\partial\boldsymbol{\nu}}(p,\phi)=0,
\end{aligned} \tag{90}$$

where $\boldsymbol{\nu}$ is the unit normal vector. The splay (14) and twist (15) constraints in terms of φ are

$$0=\nabla\cdot\mathbf{n}=\cos\varphi\varphi_\phi+\sin\varphi\cot\phi \text{ in } \Omega, \tag{91}$$

$$0=\mathbf{n}\cdot\nabla\times\mathbf{n}=\varphi_r \text{ in } \Omega. \tag{92}$$

The following theorem establishes the existence of critical points for the energy.

Theorem 11. *There exist* $\mathbf{n}=\sin\varphi\mathbf{e}_\phi+\cos\varphi\mathbf{e}_\theta$ *and free boundary functions* p *of* Ω_0 *in the set*

$$\mathcal{A}=\{(p,\varphi)\in H^1([\phi^*,\pi/2])\times H^1(\Omega):\nabla\cdot\mathbf{n}=0=\mathbf{n}\cdot\nabla\times\mathbf{n} \text{ in } \Omega, \text{ conditions (90) hold}\}$$

that minimize E_{cap}.

Proof. By the theory in §2.1, we can conclude that $\tilde{W}_{cap}$ is weak lower semicontinuous. What

remains to show the existence of minimizers is that the limit of a minimizing sequence from the admissible set $\mathcal{A}$ is itself in $\mathcal{A}$. Let (p_k, φ_k) be a minimizing sequence of $\tilde{W}_{cap}$ in $\mathcal{A}$ with weak limit (p, φ) in $H^1([\phi^*, \pi/2]) \times H^1(\Omega)$. To first address the constraints on $\mathbf{n}$, let

$$\mathbf{n}_k = \sin\varphi_k \mathbf{e}_\phi + \cos\varphi_k \mathbf{e}_\theta.$$

Because $\mathbf{n}_k$ is continuous with respect to φ_k and $\varphi_k \to \varphi$ in $L^2(\Omega)$ implies pointwise convergence almost everywhere of a subsequence (by the same name), then $\mathbf{n}_k \to \mathbf{n}$. Therefore, the constraints are satisfied by the same arguments as in Theorem 8.

Now, to show that the boundary conditions will hold, let (p^0, φ^0) be a fixed element of $\mathcal{A}$. Then $p_k - p^0 \in H_0^1([\phi^*, \pi/2])$ and $\varphi_k - \varphi^0 \in H_0^1(\Omega)$. Being that H_0^1 is a closed space, we can conclude $p - p^0 \in H_0^1([\phi^*, \pi/2])$ and $\varphi - \varphi^0 \in H_0^1(\Omega)$. Thus, the boundary conditions are satisfied, and (p, φ) is in $\mathcal{A}$. □

Of course, the energy may have many critical points. A configuration of interest in this work is the planar spooling configuration $\mathbf{n} = \mathbf{e}_\theta$, which corresponds to $\varphi \equiv 0$. This solution satisfies the boundary conditions, splay and twist constraints, and the Euler-Lagrange equations for φ (omitted), and thus, the question of whether this configuration has the least energy begs to be addressed. In Theorem 12, we show that it, indeed, does have the least energy among configurations that we consider.

This result was anticipated due to the fact that the packing is at near-crystalline density, which leaves little room for randomness in the configuration. Theoretical works done by experimentalists, such as [20, 28, 61], assume this configuration without remark. In fact, in Theorem 12, we will demonstrate that even with weaker boundary information, as long as it is satisfied by $\mathbf{n} = \mathbf{e}_\theta$, the solution $\varphi \equiv 0$ will have lower energy than a non-constant minimizer φ^*, such that $\varphi^*_\theta \equiv 0$, when each is paired with a fixed free boundary p^* that corresponds with φ^*.

Theorem 12. *The function $\varphi \equiv 0$ is the unique minimizer in $\mathcal{A}$ for a given inner boundary function p^*.*

Proof. Suppose $(p^*, \varphi^*) \in \mathcal{A}$ is a minimizing pair for $\tilde{E}_{cap}$ such that φ^* is not identically zero. Suppose also that $\varphi^*_\theta \equiv 0$. Let

$$\mathbf{n}^* = \sin\varphi^* \mathbf{e}_\phi + \cos\varphi^* \mathbf{e}_\theta. \tag{93}$$

We compare the energy for $\mathbf{n}^*$ with that of $\mathbf{e}_\theta = \sin(0)\mathbf{e}_\phi + \cos(0)\mathbf{e}_\theta$. Therefore, with the splay

and twist constraints from (91) and (92) applied,

$$\begin{aligned}\tilde{E}_{cap}(\mathbf{n}^*) - \tilde{E}_{cap}(\mathbf{e}_\theta) &= \int_\Omega K_3 \left\{ \left[1 + \left(\sin\varphi^* \varphi^*_\phi - \cos\varphi^* \cot\phi \right)^2 \right] - \left[1 + \cot^2\phi \right] \right\} \sin\phi \, dr d\phi d\theta \\ &= K_3 \int_\Omega \left[\varphi^{*2}_\phi - \left(\cos\varphi^* \varphi^*_\phi + \sin\varphi^* \cot\phi \right)^2 \right] \sin\phi \, dr d\phi d\theta \\ &= K_3 \int_\Omega |\nabla \varphi^*|^2 \, r^2 \sin\phi \, dr d\phi d\theta \\ &\geq 0,\end{aligned}$$

and only equals zero if $\varphi^* \equiv 0$. Thus, $\varphi \equiv 0$ is the unique minimizer in $\mathcal{A}$ for a given p^*. □

Therefore, what remains is to determine minimizing free boundary functions p that pair with $\varphi \equiv 0$, i.e. $\mathbf{n} = \mathbf{e}_\theta$. The energy is

$$\begin{aligned}\tilde{E}_{cap}(\mathbf{e}_\theta) &= K_3 \int_{\phi^*}^{\pi/2} \int_0^{2\pi} \int_{p(\phi)}^1 (\csc\phi - \nu r^2 \sin\phi) dr d\theta d\phi + 2\pi\sigma \int_{\phi^*}^{\pi/2} p\sqrt{p^2 + (p')^2} \sin\phi d\phi \\ &= \int_{\phi^*}^{\pi/2} \left(2\pi K_3 \csc^2\phi (1-p) - \frac{2\pi\nu}{3}(1-p^3) + 2\pi\sigma p \sqrt{p^2 + (p')^2} \right) \sin\phi d\phi. \end{aligned} \tag{94}$$

To learn about minimizers, we find the Euler-Lagrange equation for p. To do so, we take fixed $q \in H^1_0([\phi^*, \pi/2])$ and let

$$\begin{aligned} i(\epsilon) = 2\pi \int_{\phi^*}^{\pi/2} \Bigg(& K_3 \csc^2\phi (1 - p - \epsilon q) - \frac{\nu}{3}\left(1 - (p+\epsilon q)^3\right) \\ & + \sigma (p + \epsilon q) \sqrt{(p+\epsilon q)^2 + (p' + \epsilon q')^2} \Bigg) \sin\phi d\phi. \end{aligned}$$

Then,

$$i'(0) = 2\pi \int_{\phi^*}^{\pi/2} \left[-K_3 \csc^2\phi + \nu p^2 - \sigma \left(\frac{pp'}{\sqrt{p^2 + (p')^2}} \right)' + \sigma \frac{2p^2 + (p')^2 - pp'\cot\phi}{\sqrt{p^2 + (p')^2}} \right] q \sin\phi \, d\phi$$

Therefore, any minimizing p must satisfy

$$K_3 \csc^2\phi = \nu p^2 - \sigma \left(\frac{pp'}{\sqrt{p^2 + (p')^2}} \right)' + \sigma \frac{2p^2 + (p')^2 - pp'\cot\phi}{\sqrt{p^2 + (p')^2}}. \tag{95}$$

One thing to immediately notice is that the trivial free boundary $p \equiv r_0$ is not a solution to (95) because of the forcing term on the left-hand side.

8 Modifications to the Basic Models

We have seen that mechanical models of DNA clustering provide information on its packing configurations, whether in free solution or confined within viral capsids. In these models, negative electrostatic repulsion between neighboring strands of DNA have been accounted for by selecting effective parameter values, such as the diameter of the DNA and the bulk and shear moduli.

Experiments regarding the dependence on mechanical properties of single DNA molecules in an ionic environment are not ubiquitous but have a fairly long history. In their article from 1997, Baumann et al [6] studied the effect of several types of ions on the elasticity of single DNA molecules. They studied the dependence of the DNA persistence length L_p on the ionic content of the sample. They found that L_p is inversely proportional to the ionic concentration, that is, the higher the concentration, the more isotropic the behavior of the DNA. The response is also very much dependent on the ionic size. For multivalent salts, values of L_p are in the range of 25 to 30 nm, whereas for monovalent salts, L_p was found to be between 45 and 50 nm. Spermidine (a $3+$ ionic group) is found to cause larger increase of persistence length than other ionic groups like Mg^{2+}. From a different point of view, the elastic stretch modulus is found to increase with L_p, contrary to the prediction from three-dimensional elasticity.

Other groups of experimental scientists have studied the effect of ions on packing pressure and speeds of ejection, with the article by Puck and Sagic being one the pioneers in the topic [52]. The work by Purohit et al [53] provides measures of forces in the capsid with varying ionic concentration, and, in particular, during the ejection process. Fuller et al [18] investigated how ion concentration affects the functioning of the portal motor. Dogic et al [14] studied the effect of ions on the ordering of packed DNA. Analogous work for DNA in free solution was earlier carried out by [34]. How ions affect the packing energy and pressure is reported in [58].

From another perspective, ions are found to play an important role on how viruses interact with the environment and in their invasion of bacteria, as investigated in the pioneering work by Garen et al. [19]. Hence, mathematical models of ionic behavior of bacteriophage viruses are relevant to applications. Research on interactions of virus with hosts, in environments with a wide range of ionic strengths is reported in [32].

In order to study ionic effects in viruses, one approach is to model the capsid and virus, together with its surroundings as a gel. That is, the virus is placed in an aqueous environment that is able to sustain ions. Due to the permeability of the capsid, ions can then move through it and change conditions inside the bacteriophage.

8.1 An Energy for Mixing

The introduction of solvent into our model systems will be necessary to capture realistic behavior seen in experiments. The natural solvent in both LCLC and condensed DNA systems is, of course, water with immersed ions. In experiments, their concentrations are adjusted by the addition of condensing agents, such as polyethylene glycol (PEG) or spermine, these often being positive multivalent ions, to induce changes of configuration, such as shape and size of aggregates. Experimental works on LCLCs, such as [59, 60], demonstrate that the shapes of the macromolecular structures can be controlled with neutral and weakly charged additives. They observe that these additives can cause phase separations, such as the highly ordered hexagonal columnar phase coexisting with the isotropic phase.

The goal of this subsection is to model the role of condensing effects in the system, deferring the explicit electrostatic treatment to the next section. We now assume that our systems, LCLCs as well as bacteriophage viruses, are polyelectrolyte gels.

We assume that the liquid crystal occupies the domain $\mathcal{B} \subset \mathbb{R}^3$. According to the two-component mixture theory, at each point of the gel (mixture) domain, both components, liquid crystal and water are present with volume fractions ϕ_1 and ϕ_2, respectively. Assuming that no other components are present (ions and condensing agents will be represented as points, with concentrations assigned to them but occupying zero volume), we assume that the constraint

$$\phi_1 + \phi_2 = 1, \quad \phi := \phi_1, \tag{96}$$

holds. The optimal proportion of the components in the mixture is that which minimizes the Flory-Huggins energy [57], $\int_{\mathcal{B}} W_{FH}(\phi(\mathbf{x}), 1 - \phi(\mathbf{x}))\, d\mathbf{x}$, with

$$W_{FH}(\phi, 1-\phi) = \mu H(\phi), \quad \phi := \phi_1, \tag{97}$$

$$H(\phi) := \frac{N_2}{N_1}\phi \ln(\phi) + (1-\phi)\ln(1-\phi) + \frac{\chi}{2}\phi(1-\phi), \tag{98}$$

$$\mu = \frac{K_B T}{N_2 V_m}. \tag{99}$$

The first and second terms of this energy correspond to the entropic, attractive, interactive contributions between the two components, favoring their mixing; the third term represents repulsive forces between them. The Flory's parameter χ is, then, a dimensionless measure of the repulsive interactions. It has a threshold value, $\chi_c \approx 1$, such that $\chi < \chi_c$ corresponds to mixed states, with $\chi \geq \chi_c$ characterizing phase separating regimes where clusters of one component form within the second. The quantities N_1 and N_2 are the number of lattice sites occupied by species 1 and 2, respectively. (For instance, in polymer-solvent mixtures, $N_1 = 1000$, $N_2 = 1$.)

h

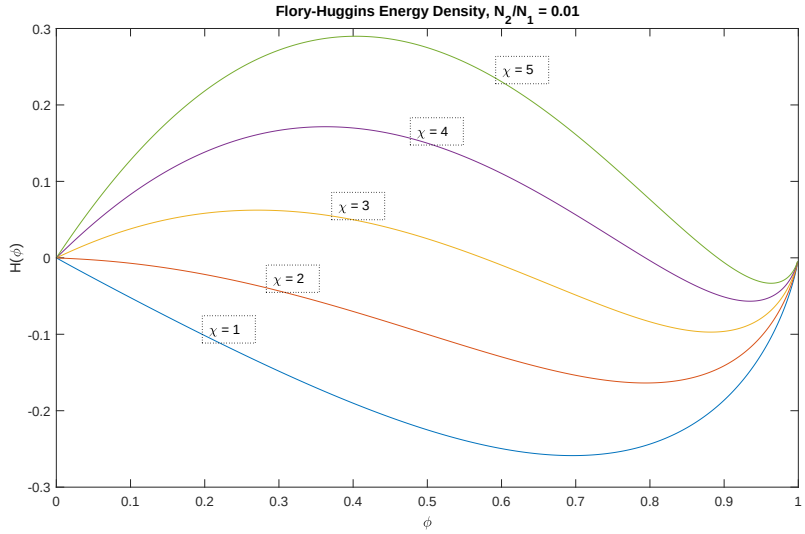

Figure 17: Profiles of the Flory-Huggins energy density for different values of χ. For $\chi > 1$, the graphs represent phase separation regimes, whereas $\chi < 1$ corresponds to a mixing regime, with a single well.

The total energy of the chromonic liquid crystal, taking into account both components, water and liquid crystal molecules is now

$$E_{mix} = \int_{\mathcal{B}} \left(\phi K_3 |\mathbf{n} \times \nabla \times \mathbf{n}|^2 + \mu H(\phi)\right) d\mathbf{x} + \sigma \, \mathrm{Area}(\partial\Omega),$$

subject to the constraints (13-16) together with

$$\int_{\mathcal{B}} \phi \, d\mathbf{x} = m, \tag{100}$$

where m represents the total mass of chromonic molecules (here we have taken the density to be 1). In the modeling of the Sunset Yellow LCLC, the bending constant is

$$K_3 = \frac{K_B T L_p}{D^2}, \tag{101}$$

where D is the typical cluster size [65], ranging from nanometers to microns according to whether we model DNA in free solution or Sunset Yellow, respectively.

8.2 Ionic Forces in Bacteriophage DNA Model

Experiments designed to understand toroidal DNA condensates, which have been motivated by relevance to gene packing and potential applications in artificial gene delivery [24], use similar condensing agents to manipulate the system. Also, experimentalists investigate the various sizes of DNA toroids that form by altering the amount of salt ions in the system, relevant due to the fact that the DNA strand carries a largely negative charge. This feature of the DNA strand also plays a major role in the setting of bacteriophage capsids, so we discuss an energy below that will encompass both the solvent and the charges of the system in that case.

When it comes to DNA spooling in bacteriophages, the inclusion of ionic forces will prove to be essential in fully understanding bacteriophage processes. For instance, the ejection behavior of virus T5 has been seen to be different from that of virus λ, which are similar in structure [43], and this suggests that more than mechanics are at play.

In this section, we explicitly account for the negative charge that we assume distributed along the DNA axis and for several families of soluble ions, which diffuse in the water contained inside the capsid and in the fluid surrounding the capsid. The permeability of the capsid walls allows for water to diffuse through, so ionic changes in the environment affect the conditions inside the capsid.

Following earlier work on polyelectrolyte gels, we now construct the energy of the present system. We consider a larger domain $\mathcal{U}$ that contains the capsid $\mathcal{B}$ to account for the permeability of the capsid walls. In addition to the orientational fields $\mathbf{n}, \mathbf{m}$ and $\mathbf{p}$ and DNA volume fraction ϕ, the model includes the diameter of the DNA d, the electrostatic potential Φ, and the concentrations $\{c_i\}_{i=1,\dots,Z}$ of the Z ion species with valence z_i. The electric displacement vector $\mathbf{D}$ is given by

$$\mathbf{D} = \varepsilon_0 \varepsilon \mathbf{E}, \quad \mathbf{E} = -\nabla \Phi, \tag{102}$$

where ε_0 is the dielectric permitivity coefficient of the vacuum and ε is the permitivity matrix of the material. Specifically,

$$\varepsilon = \varepsilon_\perp I + \varepsilon_a \mathbf{n} \otimes \mathbf{n}, \quad \varepsilon_a = \varepsilon_\parallel - \varepsilon_\perp \tag{103}$$

where $\varepsilon_\perp$ and $\varepsilon_\parallel$ denote are the permitivity coefficients when the electric field $\mathbf{E}$ is applied along the directions perpendicular and parallel to $\mathbf{n}$, respectively.

The total energy of the system is

$$E_{\text{ionic}} = E_{cap} + E_d + \int_{\mathcal{U}} [W_{FH}(\phi, 1-\phi) + \frac{1}{2}\mathbf{D} \cdot \mathbf{E} + W_{\text{ion}}(c_i)] \, d\mathbf{x} \tag{104}$$

where

$$E_d = \int_\Omega \frac{1}{\epsilon^2} |\nabla d|^2 \, d\mathbf{x} \tag{105}$$

$$W_{\text{ion}} = K_B T \sum_{i=1}^{Z} c_i \ln c_i. \tag{106}$$

$E(d)$ is a regularization term associated with the DNA interstrand distance d, and W_{ion} is the entropic energy associated with ionic concentrations. The configurations of the capsid correspond to critical points of E_{ionic} subject to constraints

$$\nabla \cdot \mathbf{D} = -\chi_{\mathcal{B}} \frac{\pi q_0 d}{4} + \sum_{i=1}^{Z} z_i c_i \text{ in } \mathcal{U}, \tag{107}$$

where $q_0 = 5.88$ e/nm is the linear charge density of the DNA. Here χ_B denotes the characteristic function of the domain $\mathcal{B}$. Taking the first variation of the energy, we recover the boundary conditions corresponding to the electrostatic contribution

$$\left[\bar{\epsilon} \frac{\partial \Phi}{\partial \boldsymbol{\nu}} \right] = 0 \text{ on } \partial\mathcal{B}, \quad \frac{\partial \Phi}{\partial \boldsymbol{\nu}} = 0 \text{ on } \partial\mathcal{U}. \tag{108}$$

The analysis of the critical points of the energy (104) follows along the steps in the analogous work on ferroelectric liquid crystals [49] and it is also related to earlier studies on polyelectrolyte gels [9, 44].

9 Concluding Remarks

The aims of this dissertation were to present a simple, user-friendly continuum model for the hexagonal phase of LCLCs and to demonstrate its utility in settings in which this phase is naturally observed. We introduced two models, one a variation of the other, that accounted for the energy of distorting the liquid crystal director, as well as the energy of interaction between adjacent phases. Constraints were imposed to enforce the lattice structure of the planes perpendicular to the director seen in the hexagonal columnar phase.

Our first study was to consider nematic liquid crystal confined between coaxial cylinders to investigate the addition of a surface energy term to the classic Oseen-Frank energy for liquid crystals. We omitted the constraints of our model for the hexagonal columnar phase. With this model, we conducted a bifurcation study on two important values of the problem: the inner cylinder radius and relative importance of surface tension versus liquid crystal moduli.

Next, we tested the predictive power our LCLC model for the hexagonal columnar phase by calculating equilibrium shapes of toroidal aggregates in two regimes, where the bending contribution to the energy dominated and where the surface forces dominated. The results were compared with experimental images of DNA toroids and LCLC toroids, respectively. This investigation concluded with a discussion of how the parameters calibrated in a simpler geometry could be used in minimizing the energy in the less restrictive geometry.

The last test case explored in this work is that of DNA confined within a bacteriophage capsid. The LCLC model for the hexagonal columnar phase was modified to also account for the energy within the disordered core region that forms at the center of capsids, due to the inability of DNA to spool indefinitely. The boundary between ordered and disordered states was taken to be an unknown function, and an existence result for simultaneously minimizing DNA configurations and the free boundary was proved. We showed that with physical boundary conditions in place, there is a unique minimizer for the DNA configuration that agrees completely with experimental images. A discussion of the associated minimizing free boundary functions followed.

The tests described above demonstrated practical applications, as well as assure well-posedness, of the models in relevant geometries. The final section provided modifications that expand the models to allow for features assumed as given to, instead, be treated as unknowns of the problem. In summary, this dissertation gives scientists and researchers a set of tools to aid with predictions and analysis of substances exhibiting the hexagonal columnar phase. With its broad scope, the hope is that scholars will pursue the potential future directions of this work and continue along this path.

References

[1] Luigi Ambrosio and Giuseppe Buttazzo. An optimal design problem with perimeter penalization. *Calculus of Variations and Partial Differential Equations*, 1(1):55–69, 1993.

[2] Javier Arsuaga, Robert K-Z Tan, Mariel Vazquez, Stephen C Harvey, et al. Investigation of viral dna packaging using molecular mechanics models. *Biophysical chemistry*, 101:475–484, 2002.

[3] Javier Arsuaga, Mariel Vazquez, Paul McGuirk, Sonia Trigueros, Joaquim Roca, et al. Dna knots reveal a chiral organization of dna in phage capsids. *Proceedings of the National Academy of Sciences of the United States of America*, 102(26):9165–9169, 2005.

[4] John M Ball. Convexity conditions and existence theorems in nonlinear elasticity. *Archive for rational mechanics and Analysis*, 63(4):337–403, 1976.

[5] Patricia Bauman, M Carme Calderer, Chun Liu, and Daniel Phillips. The phase transition between chiral nematic and smectic a* liquid crystals. *Archive for rational mechanics and analysis*, 165(2):161–186, 2002.

[6] Christoph G Baumann, Steven B Smith, Victor A Bloomfield, and Carlos Bustamante. Ionic effects on the elasticity of single dna molecules. *Proceedings of the National Academy of Sciences*, 94(12):6185–6190, 1997.

[7] F Bethuel, Haim Brezis, BD Coleman, and F Hélein. Bifurcation analysis of minimizing harmonic maps describing the equilibrium of nematic phases between cylinders. *Archive for rational mechanics and analysis*, 118(2):149–168, 1992.

[8] Mario E Cerritelli, Naiqian Cheng, Alan H Rosenberg, Catherine E McPherson, Frank P Booy, and Alasdair C Steven. Encapsidated conformation of bacteriophage t7 dna. *Cell*, 91(2):271–280, 1997.

[9] Haoran Chen, Maria-Carme Calderer, and Yoichiro Mori. Analysis and simulation of a model of polyelectrolyte gel in one spatial dimension. *Nonlinearity*, 27(6):1241, 2014.

[10] Robert J Citorik, Mark Mimee, and Timothy K Lu. Bacteriophage-based synthetic biology for the study of infectious diseases. *Current opinion in microbiology*, 19:59–69, 2014.

[11] PE Cladis and M Kleman. Non-singular disclinations of strength s=+ 1 in nematics. *Journal de Physique*, 33(5-6):591–598, 1972.

[12] Zoey S Davidson, Louis Kang, Joonwoo Jeong, Tim Still, Peter J Collings, Tom C Lubensky, and AG Yodh. Chiral structures and defects of lyotropic chromonic liquid crystals induced by saddle-splay elasticity. *Physical Review E*, 91(5):050501, 2015.

[13] *NIST Digital Library of Mathematical Functions*. http://dlmf.nist.gov/, Release 1.0.18 of 2018-03-27. F. W. J. Olver, A. B. Olde Daalhuis, D. W. Lozier, B. I. Schneider, R. F. Boisvert, C. W. Clark, B. R. Miller and B. V. Saunders, eds.

[14] Zvonimir Dogic and Seth Fraden. Ordered phases of filamentous viruses. *Current opinion in colloid & interface science*, 11(1):47–55, 2006.

[15] Masao Doi and Nobu Kuzuu. Structure of the interface between the nematic phase and the isotropic phase in the rodlike molecules. In *J. Appl. Polym. Sci.: Appl. Polym. Symp*, volume 41, pages 65–68, 1985.

[16] G Effantin, P Boulanger, E Neumann, L Letellier, and JF Conway. Bacteriophage t5 structure reveals similarities with hk97 and t4 suggesting evolutionary relationships. *Journal of molecular biology*, 361(5):993–1002, 2006.

[17] Frederick C Frank. I. liquid crystals. on the theory of liquid crystals. *Discussions of the Faraday Society*, 25:19–28, 1958.

[18] Derek N Fuller, John Peter Rickgauer, Paul J Jardine, Shelley Grimes, Dwight L Anderson, and Douglas E Smith. Ionic effects on viral dna packaging and portal motor function in bacteriophage φ29. *Proceedings of the National Academy of Sciences*, 104(27):11245–11250, 2007.

[19] Alan Garen and Theodore T Puck. The first two steps of the invasion of host cells by bacterial viruses. ii. *Journal of Experimental Medicine*, 94(3):177–189, 1951.

[20] William M Gelbart and Charles M Knobler. The physics of phages. *Physics Today*, 61(1):42–47, 2008.

[21] PG De Gennes, J Prost, and R Pelcovits. The physics of liquid crystals. *Physics Today*, 48(5):67, 1995.

[22] Paul Grayson, Alex Evilevitch, Mandar M Inamdar, Prashant K Purohit, William M Gelbart, Charles M Knobler, and Rob Phillips. The effect of genome length on ejection forces in bacteriophage lambda. *Virology*, 348(2):430–436, 2006.

[23] Robert Hardt, David Kinderlehrer, and Fang-Hua Lin. Existence and partial regularity of static liquid crystal configurations. *Communications in mathematical physics*, 105(4):547–570, 1986.

[24] Nicholas V Hud and Igor D Vilfan. Toroidal dna condensates: unraveling the fine structure and the role of nucleation in determining size. *Annu. Rev. Biophys. Biomol. Struct.*, 34:295–318, 2005.

[25] Huiqiang Jiang and Fanghua Lin. A new type of free boundary problem with volume constraint. *Communications in Partial Differential Equations*, 29(5-6):821–865, 2004.

[26] Wen Jiang, Juan Chang, Joanita Jakana, Peter Weigele, Jonathan King, and Wah Chiu. Structure of ϵ15 bacteriophage reveals genome organization and dna packaging/injection apparatus. *Nature*, 439(7076):612, 2006.

[27] John E Johnson and Wah Chiu. Dna packaging and delivery machines in tailed bacteriophages. *Current opinion in structural biology*, 17(2):237–243, 2007.

[28] James Kindt, Shelly Tzlil, Avinoam Ben-Shaul, and William M Gelbart. Dna packaging and ejection forces in bacteriophage. *Proceedings of the National Academy of Sciences*, 98(24):13671–13674, 2001.

[29] M Kleman. Developable domains in hexagonal liquid crystals. *Journal de Physique*, 41(7):737–745, 1980.

[30] Maurice Kleman and Oleg D Laverntovich. *Soft matter physics: an introduction*. Springer Science & Business Media, 2007.

[31] WS Klug and M Ortiz. A director-field model of dna packaging in viral capsids. *Journal of the Mechanics and Physics of Solids*, 51(10):1815–1847, 2003.

[32] Petra Kukkaro and Dennis H Bamford. Virus–host interactions in environments with a wide range of ionic strengths. *Environmental microbiology reports*, 1(1):71–77, 2009.

[33] Gabriel C Lander, John E Johnson, Donald C Rau, Clinton S Potter, Bridget Carragher, and Alex Evilevitch. Dna bending-induced phase transition of encapsidated genome in phage λ. *Nucleic acids research*, page gkt137, 2013.

[34] D Lang, H Bujard, B Wolff, and D Russell. Electron microscopy of size and shape of viral dna in solutions of different ionic strengths. *Journal of molecular biology*, 23(2):163–181, 1967.

[35] Amélie Leforestier and Françoise Livolant. The bacteriophage genome undergoes a succession of intracapsid phase transitions upon dna ejection. *Journal of molecular biology*, 396(2):384–395, 2010.

[36] PG Leiman, S Kanamaru, VV Mesyanzhinov, F Arisaka, and MG Rossmann. Structure and morphogenesis of bacteriophage t4. *Cellular and Molecular Life Sciences CMLS*, 60(11):2356–2370, 2003.

[37] F Livolant and Y Bouligand. Liquid crystalline phases given by helical biological polymers (dna, pblg and xanthan). columnar textures. *Journal de Physique*, 47(10):1813–1827, 1986.

[38] Fran coise Livolant. La structure cristalline liquide de ladn in vivo et in vitro., 1984.

[39] Françoise Livolant and Yves Bouligand. Double helical arrangement of spread dinoflagellate chromosomes. *Chromosoma*, 80(1):97–118, 1980.

[40] John Lydon. Chromonic liquid crystal phases. *Current opinion in colloid & interface science*, 3(5):458–466, 1998.

[41] Davide Marenduzzo, Enzo Orlandini, Andrzej Stasiak, Luca Tubiana, Cristian Micheletti, et al. Dna–dna interactions in bacteriophage capsids are responsible for the observed dna knotting. *Proceedings of the National Academy of Sciences*, 106(52):22269–22274, 2009.

[42] W. L. McMillan. Simple molecular model for the smectic a phase of liquid crystals. *Phys. Rev. A*, 4:1238–1246, 1971.

[43] Ian J Molineux and Debabrata Panja. Popping the cork: mechanisms of phage genome ejection. *Nature Reviews Microbiology*, 11(3):194–204, 2013.

[44] Yoichiro Mori, Haoran Chen, Catherine Micek, and Maria-Carme Calderer. A dynamic model of polyelectrolyte gels. *SIAM Journal on Applied Mathematics*, 73(1):104–133, 2013.

[45] VG Nazarenko, OP Boiko, H-S Park, OM Brodyn, MM Omelchenko, L Tortora, Yu A Nastishin, and OD Lavrentovich. Surface alignment and anchoring transitions in nematic lyotropic chromonic liquid crystal. *Physical review letters*, 105(1):017801, 2010.

[46] Norman H Olson, Mari Gingery, Frederick A Eiserling, and Timothy S Baker. The structure of isometric capsids of bacteriophage t4. *Virology*, 279(2):385–391, 2001.

[47] RJ Ondris-Crawford, GP Crawford, Slobodan Zumer, and JW Doane. Curvature-induced configuration transition in confined nematic liquid crystals. *Physical review letters*, 70(2):194, 1993.

[48] CW Oseen. The theory of liquid crystals. *Transactions of the Faraday Society*, 29(140):883–899, 1933.

[49] Jinhae Park and M Carme Calderer. Analysis of nonlocal electrostatic effects in chiral smectic c liquid crystals. *SIAM Journal on Applied Mathematics*, 66(6):2107–2126, 2006.

[50] Anton S Petrov, Mustafa Burak Boz, and Stephen C Harvey. The conformation of double-stranded dna inside bacteriophages depends on capsid size and shape. *Journal of structural biology*, 160(2):241–248, 2007.

[51] Peter E Prevelige. Mind the gap: How some viruses infect their hosts. *Viruses*, 2(11):2536–2540, 2010.

[52] Theodore Puck and Bernard Sagik. Virus and cell interaction with ion exchangers. *Journal of Experimental Medicine*, 97(6):807–820, 1953.

[53] Prashant K Purohit, Mandar M Inamdar, Paul D Grayson, Todd M Squires, Jané Kondev, and Rob Phillips. Forces during bacteriophage dna packaging and ejection. *Biophysical journal*, 88(2):851–866, 2005.

[54] Michael Renardy and Robert C Rogers. *An introduction to partial differential equations*, volume 13. Springer Science & Business Media, 2006.

[55] Alejandro D Rey. Liquid crystal models of biological materials and processes. *Soft Matter*, 6(15):3402–3429, 2010.

[56] Charles Rosenblatt and Nabil M Amer. Optical determination of smectic a layer spacing in freely suspended thin films. *Applied Physics Letters*, 36(6):432–434, 1980.

[57] Michael Rubinstein and Ralph H Colby. *Polymer physics*, volume 23. Oxford University Press New York, 2003.

[58] Antonio Šiber, Anže Lošdorfer Božič, and Rudolf Podgornik. Energies and pressures in viruses: contribution of nonspecific electrostatic interactions. *Physical chemistry chemical physics*, 14(11):3746–3765, 2012.

[59] L Tortora, K Kaznatcheev, and OD Lavrentovich. Lyotropic chromonic liquid crystals crowded with additives. *www. lightsource. ca*, page 7, 2011.

[60] Luana Tortora, Heung-Shik Park, Shin-Woong Kang, Victoria Savaryn, Seung-Ho Hong, Konstantine Kaznatcheev, Daniele Finotello, Samuel Sprunt, Satyendra Kumar, and Oleg D Lavrentovich. Self-assembly, condensation, and order in aqueous lyotropic chromonic liquid crystals crowded with additives. *Soft Matter*, 6(17):4157–4167, 2010.

[61] Shelly Tzlil, James T Kindt, William M Gelbart, and Avinoam Ben-Shaul. Forces and pressures in dna packaging and release from viral capsids. *Biophysical journal*, 84(3):1616–1627, 2003.

[62] René van Roij. The isotropic and nematic liquid crystal phase of colloidal rods. *European journal of physics*, 26(5):S57, 2005.

[63] Epifanio G Virga. *Variational theories for liquid crystals*, volume 8. CRC Press, 1995.

[64] E Weinan. Nonlinear continuum theory of smectic-a liquid crystals. *Archive for Rational Mechanics and Analysis*, 137(2):159–175, 1997.

[65] Shuang Zhou. Elasticity, viscosity, and orientational fluctuations of a lyotropic chromonic nematic liquid crystal disodium cromoglycate. In *Lyotropic Chromonic Liquid Crystals*, pages 51–75. Springer, 2017.